NREL/TP-411-20205 • UC Category: 1262 • DE95013124

Amorphous Silicon Research Phase 1

Annual Subcontract Report 1 August 1994 – 31 July 1995

S. Guha
United Solar Systems Corp.
Troy, Michigan

NREL technical monitor: W. Luft

National Renewable Energy Laboratory
1617 Cole Boulevard
Golden, Colorado 80401-3393
A national laboratory of the U.S. Department of Energy
Managed by Midwest Research Institute
for the U.S. Department of Energy
under contract No. DE-AC36-83CH10093

Prepared under Subcontract No. ZAN-4-13318-02

October 1995

Available to DOE and DOE contractors from:
Office of Scientific and Technical Information (OSTI)
P.O. Box 62
Oak Ridge, TN 37831
Prices available by calling (615) 576-8401

Available to the public from:
National Technical Information Service (NTIS)
U.S. Department of Commerce
5285 Port Royal Road
Springfield, VA 22161
(703) 487-4650

Preface

This Annual Subcontract Report covers the work performed by United Solar Systems Corp. for the period 1 August 1994 to 31 July 1995 under DOE/NREL Subcontract No. ZAN-4-13318-02. The following personnel participated in the research program.

A. Banerjee, E. Chen, R. Clough, T. Glatfelter, S. Guha (Principal Investigator), M. Haag, G. Hammond, K. Hoffman, M. Hopson, N. Jackett, J. Noch, T. Palmer, D. Wolf, X. Xu, J. Yang, and K. Younan.

The small-angle X-ray scattering experiments reported in Section 3 were carried out at the Colorado School of Mines by D. L. Williamson and Y. Chen, and the simulation work presented in Section 5 was done in collaboration with S. Wagner and K. Vasanth of Princeton University. We thank them for the collaborative effort. We would like to thank V. Trudeau for preparation of this report.

Table of Contents

List of Figures

List of Tables

Executive Summary

Objectives

The principal objective of this R&D program is to expand, enhance and accelerate knowledge and capabilities for the development of high-performance, two-terminal multijunction hydrogenated amorphous silicon (a-Si:H) alloy modules. The near-term goal of the program is to achieve 12% stable efficiency by 1998 using the multijunction approach.

Approach

The major effort of this program is to develop high efficiency component cells and incorporate them in the triple-junction structure to obtain the highest stable efficiency. The bulk of the effort was directed toward the middle and bottom cell structure. New and improved deposition regimes were investigated to obtain better cell performance. Fundamental studies to obtain better understanding of material and cell performance were undertaken.

Status/Accomplishments

- Several new deposition regimes/conditions were explored to investigate their effect on material/device performance. No beneficial effect on cell performance could be observed by i) ion bombardment during deposition, ii) preheating the deposition gas mixture and iii) He dilution.

- Hydrogen dilution during deposition is found to improve both the initial and stable performance of a-Si:H and a-SiGe:H alloy cells. No correlation was observed between deep defect density measured by the constant photocurrent method and cell efficiency.

- Use of Schottky barrier structure was demonstrated to be a useful tool for evaluating *p i n* solar cell performance.

- Using internal photoemission method, the electrical bandgap of microcrystalline *p* layer used in high efficiency solar cell was measured to be 1.6 eV. The band discontinuity at the microcrystalline-amorphous interface is found to be predominantly at the valence band edge. Use of these parameters in numerical simulations is found to predict solar cell performance accurately.

- New measurement techniques were developed to evaluate the interface and bulk contribution of losses to solar cell performance.

- Using the optimized component cells, a stable active-area efficiency of 11.1% was achieved in a triple-junction cell of 0.25 cm^2 area. The same cell was measured at 10.8% at NREL using a triple-source simulator. **This is the highest stable cell efficiency measured by NREL for any a-Si:H alloy cell structure.** Based on the status of the component cell performance, further improvement is expected in the stable cell efficiency with continued optimization.

- State-of-the-art single and multijunction cell structures were made and the stable active-area efficiencies measured. The best values are as follows: 1) a-Si:H single-junction – 8.8%, 2) a-Si:H/a-Si:H same gap double-junction – 10.1%, 3) a-Si:H/a-SiGe:H dual gap double-junction – 11.2%, 4) a-Si:H/a-SiGe:H/a-SiGe:H triple gap triple-junction – 11.1%. **All these results are the highest reported in the literature.**

Section 1

Introduction

This report describes the research performed during Phase I of a three-phase, three-year program under NREL Subcontract No. ZAN-4-13318-02. The research program is intended to expand, enhance and accelerate knowledge and capabilities for the development of high-performance, two-terminal multijunction hydrogenated amorphous silicon (a-Si:H) alloy modules.

It is now well recognized that a multijunction, multibandgap approach has the potential of achieving the highest stable efficiency in a-Si:H alloy solar cells. In this approach, the bandgap of the materials of the component cells is varied in order to capture a wide spectrum of the solar photons. Significant progress has been made in the development of materials and cell design in the last few years, and a stable module efficiency of 10.2% has been demonstrated over 1 sq. ft. area using a triple-junction approach in which the bottom two component cells use hydrogenated amorphous silicon-germanium (a-SiGe:H) alloy. In order to meet the Department of Energy goal of achievement of 12% stable module efficiency by 1998, it is necessary to make further improvements in each of the component cells. In this program, the scope of work includes investigations on only the middle and the bottom cells. In Task I and Task II, both a-Si:H and a-SiGe:H alloys are investigated for use in the middle cell. Task III involves investigations on the bottom cell using a-SiGe:H alloy only.

The research report describes the activities carried out in Phase I on both materials and device research. Important changes in deposition conditions which affect both the plasma and the growth chemistry have been investigated, and the results are reported in Sections 2 and 3. Specifically, in Section 2, we discuss the effect of ion bombardment and gas preheating on the performance of a-Si:H and a-SiGe:H alloy solar cells. Section 3 discusses the effect of hydrogen and helium dilution on a-Si:H and a-SiGe:H alloy materials and devices. For many material researchers, facilities may not exist for the fabrication of solar cell structures. On the other hand, use of a simple structure to evaluate the expected performance of the material for photovoltaic application is highly desirable. In Section 4, we discuss the suitability of using a Schottky barrier structure to evaluate *p i n* solar cell performance. The use of microcrystalline *p* layer has been shown to improve solar cell performance considerably. Not much information, however, is available regarding the bandgap and the location of the conduction and the valence band edges of this material. In Section 5, we present experimental results on these parameters and discuss the effect of band discontinuity at the microcrystalline-amorphous interface on the performance of solar cells. In the design of solar cells, it is important to recognize the interface and bulk parameters that contribute to solar cell performance. In Sections 6 and 7, we describe carefully-designed experiments which allow us to identify the different losses coming from the bulk and the interface. In Section 8, we discuss our current status of the performance of the component and the triple-junction cells. Future directions are outlined in Section 9.

Section 2

Effects of Ion Bombardment and Gas Preheating on a-Si:H Alloy Solar Cells

Introduction

Control of growth chemistry is known to play a very important role in improving the properties of a-Si:H and a-SiGe:H alloy materials and solar cells. Ion bombardment on film growing surface by applying an electric bias is known to be an effective way to modify the film growth mechanism. By controlling the flux and energy of impinging ions, reactive species can be energized to find a favorable site and form denser network. The effect of ion bombardment during deposition on the structural and electronic properties of a-Si:H and a-SiGe:H films has been extensively studied (Knights et al. 1979, Drevillion and Toulemonde 1985, Cabarrocas et al. 1991, Perrin et al. 1989). From the studies of optoelectronic properties of a-Si:H films deposited under a negative substrate bias, Roca i Cabarrocas et al. (Cabarrocas et al. 1991) reached the conclusion that positive ion bombardment during deposition improves film properties and films with the best electronic properties are obtained at a negative bias of 50 V. Recently, Ganguly and Matsuda reported that by applying a small positive bias to the mesh type controlling electrode in a triode configuration, hole mobility can be improved by orders of magnitude (Ganguly and Matsuda 1994). However, very little has been reported on the effect of ion bombardment on the performance of a-Si:H or a-SiGe:H solar cells.

We present a systematic study of the effect of ion bombardment on both a-Si:H and a-SiGe:H alloy solar cells. Samples were deposited by rf plasma-enhanced chemical vapor deposition under both diode and triode configurations. DC bias voltage applied to the substrates was varied from -200 to 50 V to facilitate both electron and ion bombardment.

Experimental

Both a-Si:H and a-SiGe:H single-junction *p i n* solar cells were deposited in a multichamber reactor using conventional rf plasma-enhanced chemical vapor deposition. In this study, gas mixtures of Si_2H_6+H_2 and Si_2H_6+GeH_4+H_2 were used for a-Si:H and a-SiGe:H depositions, respectively. The triode configuration was achieved by introducing a grounded high-purity metal screen to a diode system between the cathode and the substrate. Experiments on the effect of electric bias were carried out by applying a dc electric bias to the substrate in both the triode (with screen) and the diode (without screen) configurations.

Experiments include the following four cases: i) a-Si:H cells deposited in a triode mode, ii) a-SiGe:H cells in a triode mode, iii) a-Si:H cells in a diode mode, and iv) a-SiGe:H cells in a diode mode. In the cases ii) and iii), the cells were deposited on textured Ag/ZnO back reflector, and the other samples were deposited on stainless steel (ss) without any back reflector. For a-SiGe:H cells, the concentration of germanium was kept constant throughout the thickness. All the solar cells reported in this work have an active area of 0.25 cm^2.

Results and Discussions on Ion Bombardment Effect

In contrast to the effect of bias on film properties (Cabarrocas et al. 1991, Ganguly and Matsuda 1994), less significant effect is observed on solar cell performance. Generally, dc bias on the substrates changes the deposition rate in both the diode and triode configurations. Since deposition rate plays a critical role in determining cell properties (Guha et al. 1992), we adjusted the deposition conditions to obtain similar deposition rates.

Triode Configuration

The most significant effect of electric bias was observed in the case of a-Si:H cells deposited in the triode configuration. A typical example of bias effect on a-Si:H cells is shown in Table 1. Thickness and deposition rate are 3000 Å and 1.5 Å/sec, respectively. Also included in Table 1 are the blue and the red fill factors measured using narrow-band-pass filters, centered at 390 and 670 nm, respectively.

As shown in Table 1, an application of positive bias to the substrate improves both the fill factors and open circuit voltage of the cells, while applying a negative bias deteriorates the cell performance. Since the red fill factor, which is mainly determined by bulk properties of the cell, shows the largest effect, it is clear that positive ion bombardment on the growing surface is detrimental to a-Si:H cells in this deposition configuration.

In the case of a-SiGe:H cells, we found that dc bias on the substrates affects both the deposition rate and the Ge content incorporated into the cells. For a given Si_2H_6/GeH_4 ratio in a solar cell configuration, open-circuit voltages turned out to be 0.63, 0.74 and 0.79 volts, respectively, for +50, 0 and -50 volt bias. The Si_2H_6/GeH_4 ratio and rf power were adjusted to keep similar Ge content and deposition rate. As shown in Table 2, with similar Ge content (as monitored by V_{oc}) and deposition rate, the performance of the a-SiGe:H cells was hardly affected by either positive or negative bias up to a certain value. At large negative biases (-150 to -200 V), the cell performance deteriorates, as mainly reflected in the red fill factors. It should be pointed out that the average thickness of the first three samples is 2500 Å, about 10% thicker than the remaining five samples listed in Table 2.

Diode Configuration

Quite different results were observed when the screen was removed. The effect of bias on a-Si:H cells in the diode mode are shown in Table 3. Note that the bias of +50 volt increases deposition rate about 15% while -10 volt bias reduces the rate by ~10%. Except for the different rates due to the bias, there is essentially no difference in cell performance for the three a-Si:H solar cells. In the case of negative bias, only 10 volts are applied because the plasma could not be sustained with the same power at higher biases.

Similar experiments were also carried out on a-SiGe:H cells in the diode mode. In this experiment, the a-SiGe:H cells were deposited on ss without back reflectors. The thickness is around 4000 Å (power was adjusted slightly to maintain similar deposition rates). As shown in Table 4, three a-SiGe:H cells deposited under different bias voltages have very similar characteristics. In this case also, sustenance of the plasma was problematic at higher voltages and hence, the bias voltage was changed only between -15 to +15 V.

Discussions

Our results indicate that positive-ion bombardment is not beneficial to either a-Si:H or a-SiGe:H cells. On the contrary, at high biases positive ion-bombardment is found to affect the cell performance adversely. Note that these results are different from reports from Ganguly and Matsuda (Ganguly and Matsuda 1994) who reported a dramatic improvement in hole mobility of a-Si:H deposited in a triode system when a small positive bias is applied to the mesh/screen. Turner et al. (Turner et al. 1990) also reported an improvement in the quality of cathode-deposited a-SiGe:H films which they attributed to the beneficial effect of positive ion bombardment. It has been conjectured that ion bombardment may increase the adatom mobility of the impinging species giving rise to a better material.

Table 1. Bias Effect on a-SI:H Cells in Triode Configuration.

Sample No.	Bias (V)	P_{max} (mW/cm^2)	J_{sc} (mA/cm^2)	V_{oc} (volt)	FF (white)	FF (blue)	FF (red)
2636	0	6.77	10.9	0.94	0.66	0.74	0.66
2635	-50	5.68	10.1	0.91	0.61	0.72	0.60
2638	+50	7.49	10.9	0.96	0.72	0.76	0.69

Table 2. Bias Effect on a-SiGe:H Cells in Triode Configuration.

Sample No.	Bias (V)	P_{max} (mW/cm^2)	J_{sc} (mA/cm^2)	V_{oc} (volt)	FF (white)	FF (blue)	FF (red)
4232	+50	7.4	19.2	0.71	0.54	0.56	0.59
4223	0	8.2	18.9	0.74	0.58	0.60	0.61
4220	-50	7.9	19.0	0.75	0.56	0.69	0.56
4332	+50	8.2	18.7	0.74	0.60	0.68	0.61
4323	0	8.3	18.4	0.73	0.62	0.68	0.62
4329	-50	8.1	18.7	0.74	0.58	0.69	0.61
4327	-150	7.6	17.9	0.75	0.57	0.67	0.58
4328	-200	7.5	18.1	0.74	0.56	0.67	0.56

Table 3. Bias Effect on a-SI:H Cells in Diode Configuration.

Sample No.	Bias (V)	P_{max} (mW/cm^2)	J_{sc} (mA/cm^2)	V_{oc} (volt)	FF (white)	Thickness (nm)
3727	0	9.51	16.1	0.93	0.63	550
3737	+50	9.56	16.6	0.93	0.62	630
3740	-10	9.58	15.9	0.93	0.64	490

Table 4. Bias Effect on a-SiGe:H Cells in Diode Configuration.

Sample No.	Bias (V)	P_{max} (mW/cm^2)	J_{sc} (mA/cm^2)	V_{oc} (volt)	FF (white)
3746	0	6.11	15.9	0.71	0.54
3747	+15	6.16	15.5	0.72	0.55
3748	-15	6.00	15.5	0.72	0.54

We believe that the above arguments are valid only if the material quality is less than optimum. The materials used in this study have been optimized using heavy hydrogen dilution which results in a better hydrogen coverage of the growing surface giving rise to increased adatom mobility. We have shown elsewhere (Guha et al. 1995) that positive ion bombardment does indeed have a beneficial effect on a-Si:H and a-SiGe:H deposited at high rates. These materials have poorer quality since the impinging species do not have enough time to find stable sites. Ion bombardment is expected to increase the adatom mobility giving rise to a superior microstructure. This is of course accompanied by bombardment-induced defects, but for poorer quality material this is off-set by the large number of defects inherent in the material.

Note that dc bias also has effect on V_{oc} of a-Si:H cells made in the triode configuration. A difference of 50 mV in V_{oc} is observed between the cells made with +50 V and -50 V bias. Three factors may cause change in V_{oc}: a) more hydrogen incorporated into the films in the case of positive bias, b) different interface situations caused by ion bombardment, and c) improved bulk properties due to reduced ion bombardment. From Table 1 we find that the increase in V_{oc} does not cause a lowering of J_{sc} and is accompanied by an increase of FF. It therefore appears that the observed higher V_{oc} is caused by improved bulk properties of a-Si:H due to reduced ion bombardment.

Preheating Effect of Gas Mixture

In a-Si:H alloy film deposition, a certain amount of energy is needed for the species to diffuse on the growing surface to find a stable site and form a denser structure. Usually the energy for the species is supplied by heating the substrate to provide thermal energy. However, a very high substrate temperature makes hydrogen evolve from the films, which can deteriorate the a-Si:H film properties. Another way to provide the species with high thermal energy is to preheat the gas mixtures or species while the substrate temperature is held at 200 ~ 300 °C.

We have carried out two experiments to preheat either the gas mixtures or species during a-Si:H solar cell deposition. In the first, gasses were preheated by heating the gas lines, either outside or in the deposition chamber. For the second experiment, a heated metal mesh (or grid) was installed between the Al screen and the substrate to energize the species (in the triode configuration).

In the heated gas line experiment, no appreciable effect was observed. This result may be limited by the maximum temperature reached in the experiment. Another explanation is that the heated gas molecules may lose their thermal energy by colliding with the walls before they can reach the growing surface. Some typical data are shown in Table 5.

Table 5. Characterization of a-Si:H Cells Deposited with and without Preheating of Gas Mixtures. The gas line was heated by a lamp inside the deposition chamber. The cells were made on SS without back reflectors and are 2700 Å thick.

Sample No.	Pre-heating	P_{max} (mW/cm^2)	J_{sc} (mA/cm^2)	V_{oc} (V)	FF
2853	Off	6.62	9.87	0.96	0.71
2856	On	6.57	9.82	0.95	0.70

In the second experiment, either tungsten (W) mesh or W wire grid was installed between the Al screen and the substrate. The W mesh/grid is ~2 cm away from the substrate. It was verified that, without plasma, there was no deposition due to thermal decomposition by only flowing the gas mixtures through the heated W mesh or grid. By increasing the current flowing through the W grids or mesh, fill factors of a-Si:H cells appear to be slightly improved. An example is presented in Table 6. In contrast, ETL group reported that a significant improvement in a-Si:H film properties in terms of defect density was observed by constant photocurrent measurement (Ganguly et al. 1994). One may argue that if a-Si:H films are deposited at nonoptimized conditions such as at low substrate temperatures, or high deposition rates, preheating may be more effective.

Note that no effort has been made to accurately measure the temperature on the metal mesh or grid in our experiments. The current flowing through the mesh for sample 3338 was 6 A. When the current was increased to 20 A, V_{oc} dropped to 0.91 V and FF to 0.60. This indicates that at this high mesh current, there is substantial heating of the substrate. We should also mention that beyond a mesh current of 8 A, the fill factor did not improve any further. The above experiments indicate that there is indeed mesh heating; however, the beneficial effect on the cell properties is negligible.

Table 6. The Effect of Preheating Species by W Grids on a-Si:H Cells.
The cells are 3000 Å thick.

Sample No.	Pre-heating	P_{max} (mW/cm^2)	J_{sc} (mA/cm^2)	V_{oc} (V)	FF
3335	Off	7.08	10.6	0.97	0.69
3338	On	7.33	10.8	0.96	0.71

Conclusions

A systematic study of electric bias effect on a-Si:H and a-SiGe:H solar cells has been carried out in both diode and triode configurations. In the triode mode, an application of positive bias on substrate improves the performance of a-Si:H cells; zero bias gives best results for a-SiGe:H cells. In the diode mode, no appreciable bias effect is observed on both a-Si:H and a-SiGe:H alloy cells. Also no significant effect of preheating of gas mixture is observed on a-Si:H cells for both diode and triode modes.

Section 3

Effect of H_2 and He Dilution on a-Si:H and a-SiGe:H Materials and Solar Cells

Introduction

Hydrogen dilution is known to improve the material quality of a-Si:H alloys by controlling the growth kinetics (Guha et al. 1981, Tanaka and Matsuda 1987, Doughty et al. 1990). Guha et al. observed that films grown using 10% silane (SiH_4) and 90% hydrogen (H_2) exhibited improved stability against prolonged light soaking when compared with films grown using pure SiH_4 (Guha et al. 1981). We have reported that by using high hydrogen dilution with optimized preparation conditions, improved performance is achieved for both a-Si:H and a-SiGe:H solar cells (Yang et al. 1994-1, Yang et al. 1994-2).

In order to understand the physics behind the improved device performance, we have carried out extensive studies on materials properties of a-Si:H and a-SiGe:H films deposited with different levels of hydrogen dilution and at different temperatures. Material characterizations employed in this work include constant photocurrent measurement (CPM), infrared (IR) absorption, hydrogen evolution, small angle x-ray scattering (SAXS), and primary photocurrent measurements (PPC). Light-induced degradation studies on a-Si:H and a-SiGe:H solar cells with different levels of hydrogen dilution have also been carried out. Also presented are preliminary experimental results on He dilution effect on a-Si:H alloy solar cells.

Experimental

In the studies on hydrogen dilution effect, Si_2H_6-H_2 and Si_2H_6-GeH_4-H_2 gas mixtures were used to deposit a-Si:H and a-SiGe:H films, respectively. Two Si_2H_6/H_2 ratios and two substrate temperatures were used for a-Si:H deposition, while a-SiGe:H films were deposited at 300 °C with two levels of hydrogen dilution. The films were grown on 7059 glass for optical and electrical characterization, on crystalline Si (c-Si) for infrared analysis, on stainless steel (ss) and c-Si for hydrogen evolution, and on Al foil for small angle x-ray scattering measurements.

Both a-Si:H and a-SiGe:H single-junction *p i n* solar cells were deposited on ss without any back reflector. The thicknesses of the intrinsic layers are ~5000 Å and ~4000 Å for a-Si:H and a-SiGe:H solar cells, respectively. For stability studies, the cells were exposed to one sun white light in open-circuit mode at 50 °C for over 1000 hours.

Results of H_2 Dilution Effect

The main characteristics of six a-Si:H and a-SiGe:H samples used in this work are listed in Table 7. Except for sample #3, all the other a-Si:H samples have similar values of dark-conductivity, σ_d, (~1×10^{-11} s/cm), and electron mobility-life time product, $\mu\tau$, measured with a flux of 5×10^{15} photons/cm^2 at 650 nm. High hydrogen diluted samples show slightly larger values of activation energy (E_a) of dark conductivity and broader optical ("Tauc") gap (E_{opt}). Similar trend is also observed for a-SiGe:H films where the high hydrogen diluted sample shows slightly higher E_a, $\mu\tau$ and E_{opt}.

Table 7. Main Characteristics of a-Si:H and a-SiGe:H Films.

Sample No.	E_{opt}(eV)	C_H(%)	E_a(eV)	σ_D ($\Omega^{-1}cm^{-1}$)	$\mu\tau$ (cm^2V^{-1})	Notes
#1	1.72	8.1	0.97	1.1e-11	1.3e-6	a-Si:H, 300 °C, low H_2 dilution
#2	1.74	7.4	1.00	0.9e-11	1.0e-6	a-Si:H, 300 °C, high H_2 dilution
#3	1.77	13.2	0.93	1.3e-10	0.9e-6	a-Si:H, 175 °C, low H_2 dilution
#4	1.79	12.3	1.04	1.1e-11	1.6e-6	a-Si:H, 175 °C, high H_2 dilution
#5	1.40	6.4	0.71	2.4e-9	1.3e-7	a-SiGe:H, 300 °C, low H_2 dilution
#6	1.43		0.79	1.2e-9	2.1e-7	a-SiGe:H, 300 °C, high H_2 dilution

Sub-bandgap Absorption

Sub-bandgap absorption measured by CPM on the films prepared under different conditions shows little difference (within measurement error). All the four a-Si:H samples had similar Urbach energy of 47 to 49 meV. The sub-bandgap absorption data are summarized in Table 8. In the initial state, the defect density for films deposited at a given temperature is within a factor of 2 from each other; the values are even closer for the degraded state. However, spectral response measured by PPC on the four a-Si:H solar cells shows larger difference in the light-soaked state with sample #3 (deposited at 175 °C with low dilution) showing the highest defect density.

Table 8. Data Obtained from CPM and PPC.

Sample No.	E_u (meV) (CPM)	$N_{s,initial}$ (CMP) (cm^{-3})	$N_{s,degraded}$ (CPM) (cm^{-3})	$QE(1.2eV)_{initial}$ (PPC) (a.u.)	$QE(1.2eV)_{degraded}$ (PPC) (a.u.)
#1	47	2.9e15	2.9e16	1.1	8.1
#2	47	4.4e15	3.0e16	1.0	5.8
#3	49	7.9e15	3.0e16	1.1	14.8
#4	48	5.0e15	2.5e16	1.0	6.2
#5	52	6.4e15			
#6	52	4.0e15			

IR Analysis

As shown in Table 7, total hydrogen concentrations (determined from 630 cm^{-1} mode) for the a-Si:H films for the two different dilutions are very similar. However, IR spectra in the range of 800 to 960 cm^{-1} reveal dramatic differences. Figure 1 compares IR absorption spectra in this range for the four a-Si:H samples. For all the samples, there is an absorption peak around 880 cm^{-1} which can be attributed to the bending mode of SiH_2 (Knights et al. 1978). However, sample #3 shows a doublet at 880 and 845 cm^{-1} indicating presence of $(SiH_2)_n$ in this sample. Note that sample #4 shows an absorption peak around 915 cm^{-1} to which we do not have satisfactory attribution.

Hydrogen Evolution

For a-Si:H samples, hydrogen evolution experiments show that there are sharp peaks at low temperature for the samples prepared with high H_2 dilution. For the pair of a-Si:H samples deposited at 300 °C, as shown in Fig. 2, sample #1 shows a main peak around 500 °C, while sample #2 has a strong and sharp peak around 400 °C. For the other pair of a-Si:H samples deposited at 175 °C, low dilution one (#3) shows three small peaks from 400 to 600 °C and the high dilution sample (#4) shows two sharp peaks around 400 and 500 °C.

In contrast to a-Si:H, there is no appreciable difference in hydrogen evolution spectra for a-SiGe:H samples deposited with low and high H_2 dilution. Both samples show a broad peak between 350 to 550 °C with three fine structures at ~380, 440 and ~480 °C.

SAXS

The SAXS data show that high H_2 dilution tends to form more anisotropic microstructure with columns parallel to the growth direction. The SAXS of the a-Si:H sample deposited at 175 °C with low H_2 dilution (#3) is isotropic, and can be modeled with spherical voids averaging near 1 nm in diameter, while the SAXS data for the other three a-Si:H samples (#1, #2 and #4) are anisotropic, showing columnar-like microstructures (Williamson 1995).

In the case of a-SiGe:H films, both the samples show columnar-like features in SAXS data. However, the sample made with high dilution exhibits stronger tilting effect than the sample made with low dilution, which indicates the existence of larger size of oriented microstructures in the high dilution sample.

Stability of Solar Cells

Both a-Si:H and a-SiGe:H cells deposited with high hydrogen dilution not only show improved performance in the initial state but also maintain superior performance in the light-soaked state. The characteristics of six solar cells with i-layers deposited under nominally identical conditions to the six samples in Table 7 are presented in Table 9. It can be seen that the a-Si:H cell deposited at 175 °C with low hydrogen dilution degraded by 43%, much more than the other three a-Si:H cells (16 to 23%). High hydrogen dilution has similar effect on a-SiGe:H solar cells. The high dilution sample has superior performance in the initial state and is also more stable than the low dilution sample.

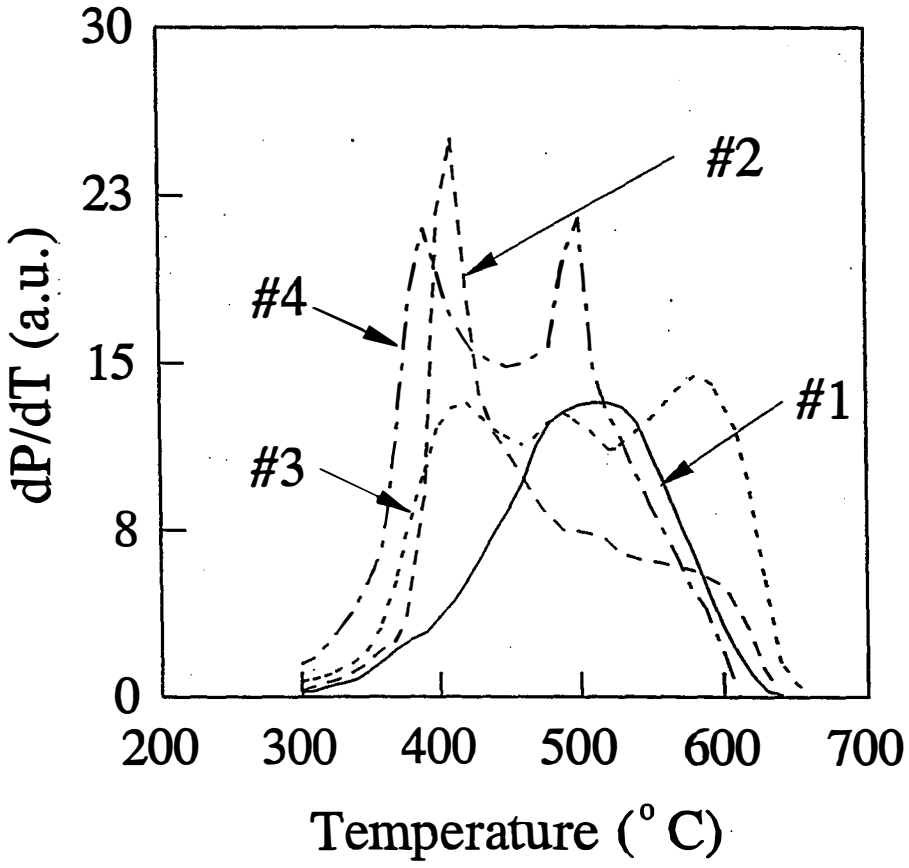

Figure 1. **IR spectra of four a-Si:H samples.**
Refer to Table 7 for sample description.

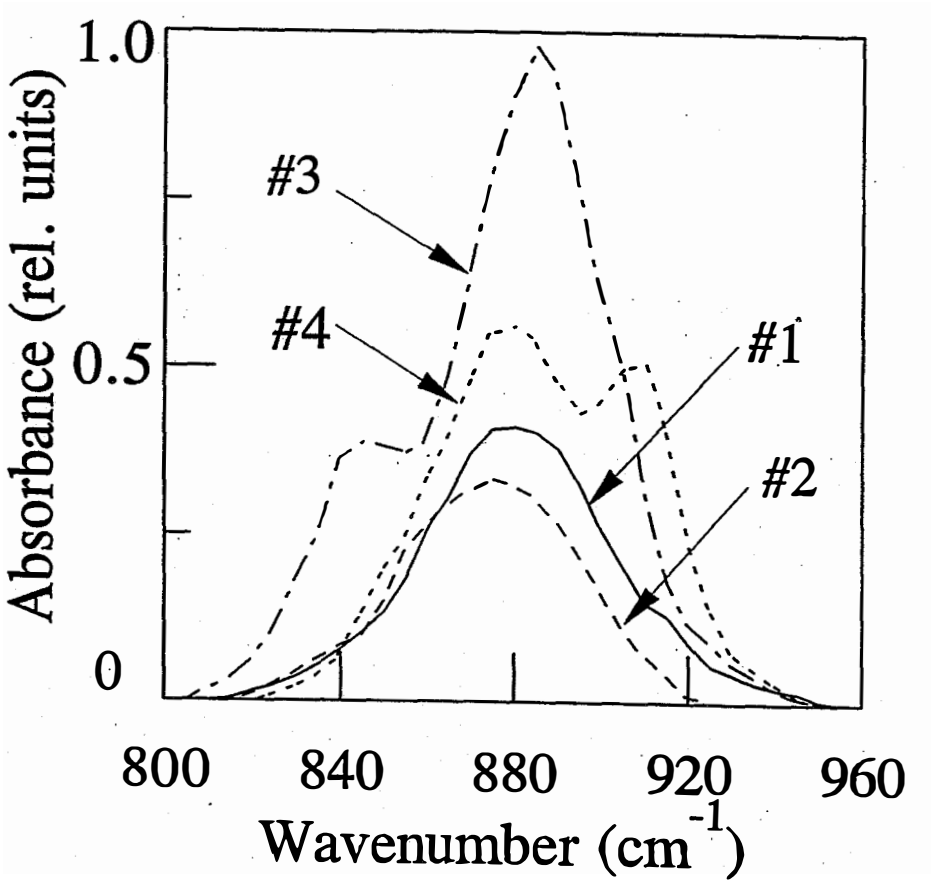

Figure 2. Hydrogen evolution spectra for four a-Si:H samples. Refer to Table 7 for sample description.

Table 9. Characteristics of a-Si:H and a-SiGe:H Cells In Both Initial and Degraded States.

Description	State	J_{sc} (mA/cm^2)	V_{oc} (volt)	FF	P_{max} (mW/cm^2)
300 °C, Low Dilution	Initial	12.3	0.94	0.65	7.5
	Degraded	11.6	0.91	0.55	5.8
	% Degradation				23
300 °C, High Dilution	Initial	11.6	0.96	0.68	7.6
	Degraded	11.2	0.94	0.61	6.4
	% Degradation				16
175 °C, Low Dilution	Initial	11.4	0.96	0.64	7.0
	Degraded	9.5	0.91	0.46	4.0
	% Degradation				43
175 °C, High Dilution	Initial	10.9	1.00	0.69	7.5
	Degraded	10.5	0.97	0.60	6.1
	% Degradation				19
a-SiGe:H, Low Dilution	Initial	17.6	0.72	0.55	7.1
	Degraded	14.9	0.64	0.41	3.9
	% Degradation				45
a-SiGe:H, High Dilution	Initial	18.0	0.74	0.59	8.0
	Degraded	16.3	0.69	0.45	5.1
	% Degradation				36

Discussions on H_2 Dilution

As the H_2 dilution ratio during a-Si:H film deposition increases, more oriented microstructures are created while the density of isotropic nanovoids (~ 1 nm in diameter) is reduced (more significantly in the low temperature case). Hydrogen associated with these oriented microstructures in high H_2 dilution samples tends to evolve out within a narrow temperature range at low temperature, corresponding to sharp peaks observed around 400 °C in H_2 evolution spectra of samples #2 and 4. However, these hydrogen atoms are not bonded in $(SiH_2)_n$ structures since in IR spectra the high dilution samples show less signals at 845 cm^{-1} and 880 cm^{-1} than the low dilution samples. The only exception is sample #1 (300 °C, low H_2 dilution); there is no low temperature peaks observed in H_2 evolution experiment although this sample does show evidence of oriented microstructures.

Correlation between SAXS data and solar cell performance is worthy of more discussions. It has been found that nanostructure in the form of 1 to 4 nm voids or H-rich clusters are harmful to solar cell performance (Knights et al. 1978, Williamson 1995). Williamson suggested that since the oriented microstructures observed in high H_2 dilution samples are parallel to the solar cell transport direction, they may not be detrimental to cell performance. However, why does the existence of these oriented microstructures improve the cell performance, particularly in the degraded state? Of particular importance is to clarify whether high hydrogen dilution creates more ordered microstructures which may enhance the transport properties in solar cells.

Regarding the sub-bandgap absorption of a-Si:H material and solar cell performance, there is still no satisfactory correlation. We have previously reported on the lack of correlation between CPM data and solar cell performance (Guha et al. 1992, Xu et al. 1993). Although PPC results showed a better correlation with cell performance, more experiments will be necessary before PPC can be used as a tool for cell evaluation.

He Dilution Effect on a-Si:H Cells

It has been reported that highly photosensitive low bandgap (~1.5 eV) a-Si:H alloy can be obtained by using helium dilution of process gases in plasma-enhanced CVD in a certain optimum pressure range (Hazra et al. 1995). Low bandgap of a-Si:H alloy films was said to be caused by reducing the bonded hydrogen content. Compared with a-SiGe:H alloy film with similar bandgap, low bandgap a-Si:H alloy films showed higher $\mu\tau$ product and photosensitivity values (Hazra et al. 1995).

We have carried out experiments to study the effect of He dilution on a-Si:H alloy solar cells. Characteristics and deposition parameters for He-diluted a-Si:H alloy cells are summarized in Table 10. The only change in deposition parameters for all the runs is the pressure which varied from 0.8 to 2.0 torr. The deposition rate increases from 0.80 Å/s to 1.7 Å/s as the pressure increases from 0.8 to 1.6 torr and comes down slightly to 1.4 Å/s at 2.0 torr. Up to 1.8 torr, there is essentially no difference in V_{oc}, and the variation in FF is caused by the difference in thickness. However, the cell deposited at 2.0 torr shows poorer FF and slightly lower V_{oc}, which indicates that the quality of the material is inferior.

In order to find out whether He dilution affects the bandgap of a-Si:H alloy film, we deposited He-diluted a-Si:H alloy films on glass substrate at different pressures. The difference in optical gap for these three a-Si:H alloy films deposited at 1.2, 1.8 and 2.00 torr is less than 0.04 eV (1.72~1.76 eV). This is consistent with the results of cells listed in Table 10 where we find only small changes in the magnitude of V_{oc}.

Except for different deposition rate and inferior performance at the highest pressure, He dilution has no effect on a-Si:H alloy solar cells made in our conventional rf PECVD system. The optical gap remains to be around 1.74 eV. However, geometrical factors of electrodes such as electrode configuration and separation may play an important role in a-Si alloy film deposition. Without knowing the geometry of the system used in the work of Hazra et al. (Hazra et al. 1995), we can not make a definite conclusion about those results of He dilution effect on a-Si:H alloy film performance.

Table 10. Characteristics of He-diluted a-Si:H Cells Deposited at Different Pressures.

Run No.	Pressure (torr)	J_{sc}	V_{oc}	FF	d(Å)	Dep.Rate (Å/s)
4747	0.8	12.4	0.93	0.68	1900	0.79
4711	1.2	14.1	0.94	0.65	2700	1.1
4720	1.6	14.4	0.93	0.58	4100	1.7
4712	1.8	15.3	0.93	0.59	3800	1.6
4715	2.0	14.6	0.89	0.42	3300	1.4

Conclusions

Our results show that measurements on a-Si:H and a-SiGe:H films in the co-planar configuration, such as $\mu\tau$ product and CPM, are not sufficient to predict solar cell performance which depends mainly on properties in the transverse direction. The existence of the oriented microstructures associated with low-temperature hydrogen evolution in both high H_2 dilution a-Si:H and a-SiGe:H materials is not necessarily deleterious to solar cell performance. In fact cells made with high H_2 dilution show the best stable performance. He dilution is found to have no effect on the optical gap of a-Si:H alloys. In contrast to expectation from published work (Hazra et al. 1995), a-Si:H films grown under He-dilution do not seem to have the desired quality to be used for low bandgap component cells.

Section 4

Evaluation of Solar Cell Performance Using Schottky Barrier Structure

Introduction

Measurement of film properties to predict device performance has been a long-desired goal for many a-Si:H alloy material researchers. Although a variety of techniques has emerged, it has been our view that measurements of film properties alone are not adequate to predict cell performance accurately. There are two reasons that contribute to this inaccuracy: (i) One needs to obtain information about both mobility and lifetime of the electrons and holes in order to predict cell performance. Film measurements do not give all the information, and (ii) the properties in the transverse direction (cell structure) may be quite different from those in the coplanar direction (film structure). We have also argued that the inherent inaccuracy of obtaining defect density from many of the film measurements (a factor of 2 to 3) will lead to uncertainties in the prediction of cell performance by 10 to 15%. A 10% difference in cell performance is, of course, significant when one is trying to achieve the world's highest efficiency.

While we believe that the best way to qualify a material for optimum device performance is to make a simple device (*p i n*) on a specular substrate, we have also been investigating other structures to assess their suitability for material qualification. The motivation has been to assist material researchers who do not have the facilities for making *p i n* cell structures. We have used a simple Schottky structure Pd (50% T)/undoped a-Si:H/n^+ a-Si:H/stainless steel to correlate the device performance with that of a solar cell with ITO/*p i n*/stainless steel configuration.

Results and Discussion

The intrinsic layers used in this study, typically 4500 Å thick, were deposited under two different conditions to provide different cell performance. All other parameters were kept the same. Table 11 shows the performance under global AM1.5 illumination of the *p i n* cells for the two deposition conditions. It is apparent that *p i n* II has poorer performance than *p i n* I; the fill factor (FF) is lower. The difference in fill factor is not as much for the Schottky structure (Table 11). In a Schottky device, the blue response is dominated by back diffusion which, in turn, is governed by the metal-semiconductor interface and is less dependent on the bulk properties. The red response, however, is more dependent on the bulk properties, and we have therefore measured the red response for the cells with suitable red filters and lenses so as to obtain short-circuit current density in the 11-12 mA/cm^2 range (as obtained for global AM1.5 illumination in the *p i n* structure). The results are shown in Table 12. We now find significant change in FF for both the *p i n* and the Schottky structure for the two cases. For the *p i n* structure, FF changes from 0.623 to 0.492 whereas for the Schottky structure, the change is from 0.604 to 0.503.

We thus believe that measurements of cell performance of Schottky diodes under red light with high intensity so as to give ~12 mA/cm^2 of short-circuit current density can be used to evaluate the quality of the *i*-layer in a *p i n* configuration. Further experiments with materials deposited under different conditions and also with Ge-incorporation are being planned to ascertain the reliability of this technique.

Table 11. Performance of Schottky and *p i n* Devices under Global AM1.5 Illumination.

	V_{oc} (V)	J_{sc} (mA/cm^2)	FF	P_{max} (mW/cm^2)
p i n I	0.943	12.6	0.692	8.22
p i n II	0.917	12.5	0.613	7.01
SB I	0.573	5.9	0.603	2.04
SB II	0.570	5.8	0.586	1.94

Table 12. Performance of Schottky and *p i n* Devices under Red (λ>610 nm) Illumination.

	V_{oc} (V)	J_{sc} (mA/cm^2)	FF	P_{max} (mW/cm^2)
p i n I	0.926	12.4	0.623	7.14
p i n II	0.891	12.6	0.492	5.51
SB I	0.579	11.7	0.604	4.08
SB II	0.567	11.5	0.503	3.28

Section 5

Band Discontinuity Effect on a-Si:H and a-SiGe:H Solar Cells

Introduction

Microcrystalline (μc) boron-doped silicon layers (Guha et al. 1986) play a key role in the improvement of the efficiency of a-Si:H alloy cells. As compared to their amorphous counterpart, μc *p*-type layers show lower conductivity activation energy and higher optical transmission, giving rise to higher open-circuit voltage (V_{oc}) and short-circuit current density (J_{sc}) for the solar cell. The properties of the thin *p*-type μc layer used in the cell, however, are not very well understood. Specifically, not much information is available regarding the bandgap of the layer and the band edge discontinuities at the *p*(μc)-intrinsic(*i*) a-Si:H alloy interface. This information is extremely important for reliable numerical simulation of the device performance starting from fundamental material parameters.

Although very little information is available regarding the μc-Si:H/a-Si:H interface, several contradictory reports have been made on the band edge discontinuities between crystalline silicon (c-Si) and the a-Si:H alloys (Evangelisti 1985, Matsuura and Okushi 1992, Mimura and Hatanaka 1987, Cuniot and Marfaing 1988). From the measurement of the internal photoemission (IPE) at a c-Si/a-Si:H alloy heterojunction, Mimura and Hatanaka (Mimura and Hatanaka 1987) concluded that the major band edge discontinuity occurs in the valence band (ΔE_v = 0.71 eV), while it is only 0.09 eV in the conduction band (ΔE_c). Cuniot and Marfaing (Cuniot and Marfaing 1988), on the other hand, used a structure of c-Si/sputtered a-Si:H alloy for IPE measurement and found that the discontinuity in the valence band is negligible, with the main discontinuity existing in the conduction band. We take ΔE_v to be positive when the valence band edge for μc- or c-Si lies above that for a-Si:H or a-SiGe:H in the electron energy diagram (Fig. 3). The opposite is the case for ΔE_c; i.e., ΔE_c is positive when the conduction band edge for μc- or c-Si lies below that for a-Si:H or a-SiGe:H (Fig. 3). We present new experimental results of IPE measurements on μc-Si:H/a-Si:H alloy structures and discuss the effect of band edge discontinuities on a-Si:H and a-SiGe:H solar cell performance.

Experimental

The samples for the internal photoemission measurement were deposited on specular stainless steel (ss) substrates without back reflectors. The structure of samples used to measure ΔE_v is ss/*p* μc-Si:H (600 Å)/*i* a-Si:H (100 - 400 Å)/*n* a-Si:H (~100 Å) (#1 and 2 of Table I3). The intrinsic a-Si:H layer was grown by rf plasma-enhanced chemical vapor deposition using a disilane-hydrogen mixture. Hydrogen diluted silane was used for μc-Si:H layer deposition. BF_3 and PH_3 were added as dopants for *p* and *n* type doping, respectively.

A semitransparent Au or Al front electrode was evaporated on top of the sample to form an Ohmic contact. The monochromatic exciting light of varying wavelength was incident on the front metal electrode. A reverse bias of 50 mV was applied for collecting the photo-generated carriers.

For cell performance studies, a-Si:H and a-SiGe:H alloy solar cells were deposited on ss substrates without back reflectors. The structure of the cells is ss/*n*/*i* a-Si:H (or a-SiGe:H)/*p* μc-Si:H/ITO. The thicknesses of the intrinsic layers are 5000 and 3700 Å for a-Si:H and a-SiGe:H cells, respectively.

Table 13. Sample Structures for Internal Photoemission Measurement and Observed Threshold Energies.

Sample No.	Structure	E_t (eV)
1	ss/*p* μc-Si:H (600 Å)/*i* a-Si:H (400 Å)/*n* a-Si:H (100 Å)/Au	1.68
2	ss/*p* μc-Si:H (600 Å)/*i* a-Si:H (100 Å)/*n* a-Si:H (100 Å)/Au	1.57
3	ss/*n* a-Si:H (200 Å)/*i* a-Si:H (1000 Å)/*p* μc-Si:H (100 Å)/ITO	1.74
4	ss/*n* μc-Si:H (600 Å)/*i* a-Si:H (100 Å)/*p* μc-Si:H (100 Å)/Al	1.85

Determination of ΔE_v and ΔE_c

According to Kane's model (Kane 1962) for indirect transitions from semiconductors, the quantum yield Y of internal photoemission in the vicinity of the threshold energy (E_t) can be expressed as

$$Y \sim (h\nu - E_t)^{5/2} \quad (1)$$

where $h\nu$ is the energy of photons. The internal photoemission process in the ss/*p* μc-Si:H/*i* a-Si:H/*n* a-Si:H/Au sample can be described as follows. The photons that are transmitted through the metal electrode and the thin *n* and *i* layers are partially absorbed in the μc-Si:H layer. The electrons are photoemitted from the valence band of μc-Si:H to the conduction band of a-Si:H (see Fig. 3). The threshold energy, E_{t1}, is the sum of the bandgap, E_g (μc-Si:H), of μc-Si:H, and ΔE_c. Since both *i* and *n* layers are very thin, the predominant contribution to the photocurrent is due to the transition from the valence band of μc-Si:H to the conduction band of the intrinsic a-Si:H alloy.

The 2/5 power of the photoemission quantum yield Y is plotted against the photon energy in Fig. 4 for two samples with different thicknesses of the intrinsic a-Si:H layer (#1 and 2 of Table 13). As seen in Fig. 4, $(Y)^{2/5}$ becomes more linear with $h\nu$ when the *i* a-Si:H layer becomes thinner. For sample #2 with a 100 Å thick *i* layer, a good linear relationship is observed in the range of 1.7 to 2.4 eV. The threshold energy, E_{t1}, is obtained by extrapolating the straight line to the intercept; and 1.57 eV is obtained for sample #2. For the sample with the 400 Å thick *i* a-Si:H layer (sample #1), the contribution of the photogenerated carriers from the *i* layer is not negligible and the intercept energy shifts to around 1.68 eV, which is close to the "threshold energy" of 1.74 eV obtained from 1000 Å thick *i* layer using the configuration of sample #3, i.e., simply the gap energy of a-Si:H.

We performed similar experiments to determine the discontinuity of the conduction band edge between μc-Si:H and a-Si:H layers using the structure #4 of Table 13, ss/*n* μc-Si (600 Å)/*i* a-Si:H (100 Å)/*p* μc-Si (100 Å)/Al. In this case, the threshold energy corresponds to the transition from the top of the valence band of a-Si:H to the bottom of the conduction band of *n* μc-Si:H. This threshold energy, E_{t2}, which is the sum of E_g(μc-Si:H) and ΔE_v, is ~1.85 eV (see Fig. 4).

The discontinuities in both the valence and the conduction band edges between μc-Si:H and a-Si:H can be determined if the value of the mobility gap of a-Si:H is known. Lee et al. measured the mobility gap by internal photoemission (Lee et al. 1990). Chen and Wronski reinterpreted these data and recommended a value for the mobility of 1.83 eV (Chen and Wronski, to be published). Using the values of E_{t1} and E_{t2} obtained from Fig. 4, we can calculate that

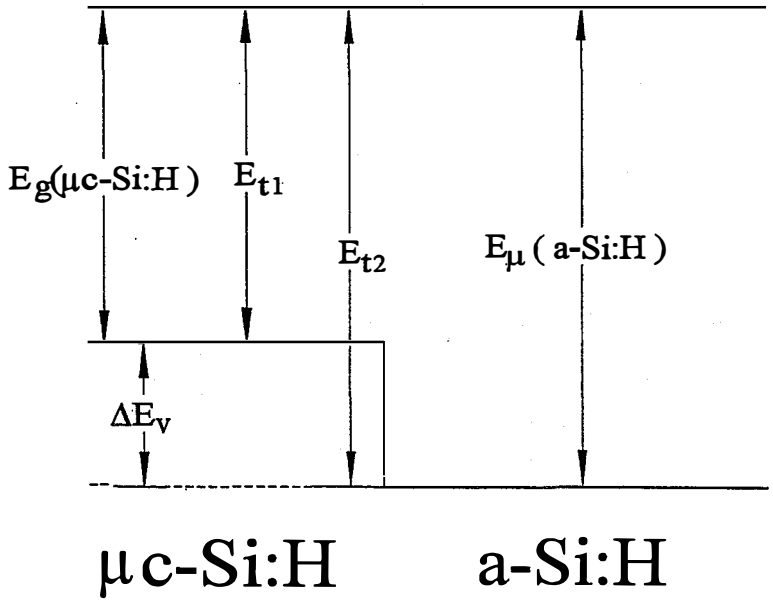

Figure 3. Schematic band diagram of the μc-Si:H/*i* a-Si:H heterostructure.

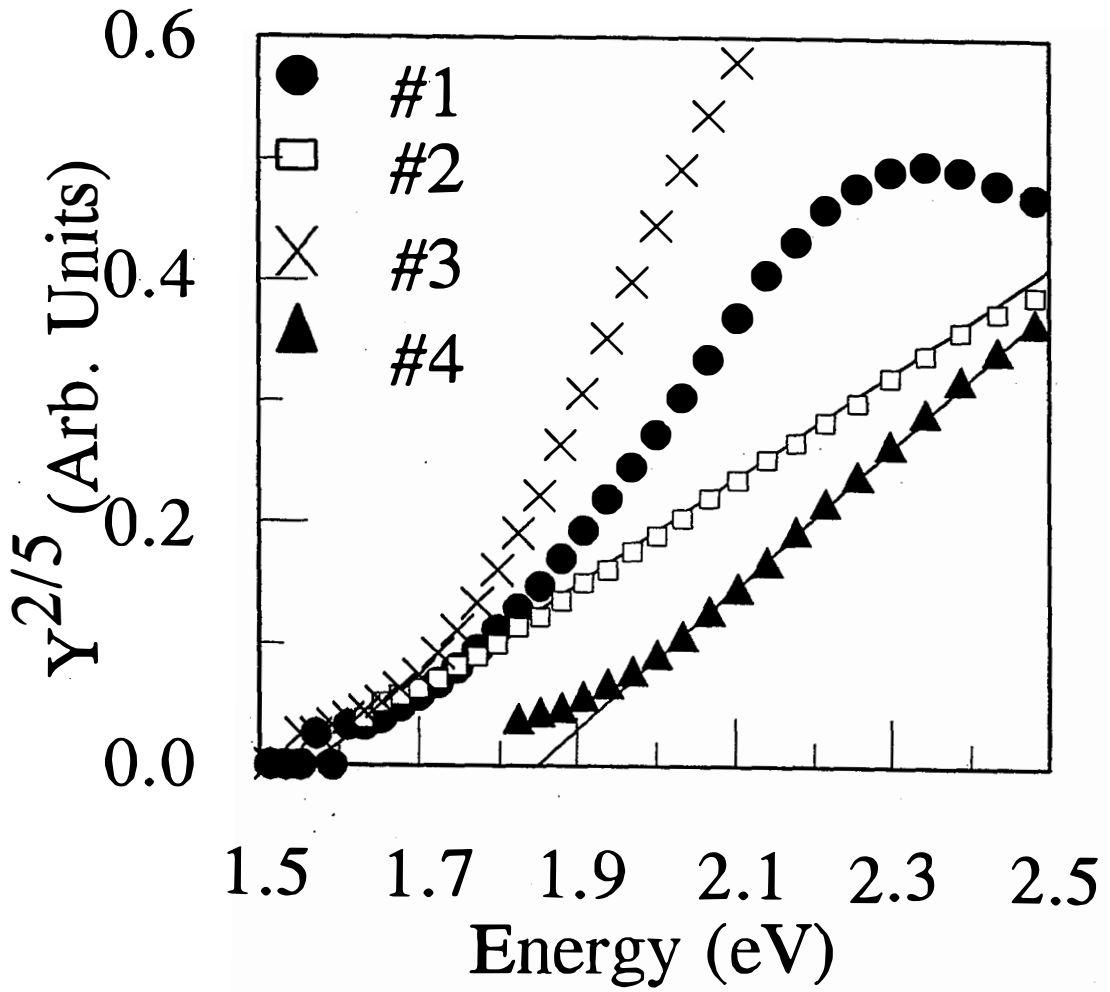

Figure 4. **$(Y)^{2/5}$ versus photon energy $h\nu$ for four samples.** The lines are eye guide.

$$\Delta E_v = E_\mu(\text{a-Si:H}) - E_{t1} = 1.83 - 1.57 = 0.26 \text{ eV} \quad (2)$$
$$\Delta E_c = E_\mu(\text{a-Si:H}) - E_{t2} = 1.83 - 1.85 = -0.02 \text{ eV} \quad (3)$$
$$E_g(\mu\text{c-Si:H}) = E_\mu(\text{a-Si:H}) - \Delta E_c - \Delta E_v = 1.83 + 0.02 - 0.26 = 1.59 \text{ eV} \quad (4)$$

The observation of an electrical bandgap of ~1.6 eV for the μc-Si:H merits some discussion. Single crystal silicon has a bandgap of 1.1 eV. It is, however, well known that for nano-crystalline silicon the bandgap increases as the cluster size decreases (Delley and Steigmeier 1993). Our earlier studies on μc-films using transmission electron microscopy (TEM) show a grain size between 70-100 Å and a crystalline volume fraction of 80%. Reflection high energy electron diffraction (RHEED) studies also confirm the existence of microcrystallinity in the thin p layers used in *p i n* solar cell configuration. Using the theoretical calculation of Delley and Steigmeier (Delley and Steigmeier 1993), who computed the bandgap of nano-crystalline Si as a function of cluster diameter using the density-functional approach for finite structures, we find a bandgap in the range of 1.5 to 1.6 eV for a cluster size of 70 Å. This value is in good agreement with our observations.

Effect on a-Si:H Cells

To study the effect of band edge discontinuities on a-Si:H and a-SiGe:H alloy solar cells with *p* μc-Si:H layers, we have carried out numerical simulations using the AMPS model developed at Penn State University (Arch et al. 1991). Calculated a-Si:H cell characteristics are tabulated in Tables 14 and 15, and compared with experimental results. Table 14 shows that V_{oc} increases (i) as the bandgap of the microcrystalline material increases and (ii) as the discontinuity at the valence band edge decreases. This is understandable since, in both of these cases, the built-in potential increases. We also find very good agreement between theory and experiment (case #3) when the measured values of E_g, ΔE_v, and ΔE_c, as obtained from the IPE measurements, are used in the numerical simulations.

Table 14. Simulated and Measured a-Si:H Alloy Cell Characteristics. A value of 1.83 eV is used for the mobility gap of a-Si:H in the simulation.

E_g(μc-Si:H) (eV)	$\Delta E_c/\Delta E_v$ (meV)	V_{oc} (V)	FF	Case #
1.90	-35/-35	0.99	0.69	1
1.59	240/0	0.98	0.68	2
1.59	0/240	0.93	0.66	3
1.10	60/670	0.53	0.59	4
Measured		0.93	0.65	

Table 15 shows the effect of bandgap of the *p* μc-Si:H layer and the band edge discontinuities on the ratio of quantum efficiency, i.e., quantum efficiency under -3 V bias to that without bias, Q(-3 V)/ Q(0V), which reflects the loss of carrier collection (Banerjee et al. 1995). In this case also, use of a bandgap of 1.1 eV (that for crystalline silicon) gives a poor fit to the experimental results. The best fit is obtained when the bandgap is taken to be 1.59 eV, and the band discontinuity is assumed to be in the valence band (case #3). This is consistent with the results from IPE measurement.

Table 15. Ratio of Q(-3 V), Quantum Efficiency under -3 V Bias, to Q(0 V), with No Bias, for a-Si:H Cells as a Function of Wavelength.

E_g(μc-Si:H) (eV)	$\Delta E_c/\Delta E_v$ (meV)	λ (nm)	[Q(-3 V)/Q(0 V) - 1]×100 (%) 400	500	600	700	Case #
1.90	-35/-35		1.4	0.9	2.5	5.9	1
1.59	240/0		2.0	1.1	2.5	5.8	2
1.59	0/240		9.9	3.8	3.4	6.7	3
1.10	60/670		65.8	21.2	10.5	14.6	4
Measured			6.6	2.2	2.5	5.8	

Effect on a-SiGe:H Cells

Simulated and measured values of a-SiGe:H alloy cell characteristics are summarized in Tables 16 and 17. The optical gap of the a-SiGe:H alloy was measured to be 1.55 eV. In the simulation, a mobility gap of 1.63 eV is used for a-SiGe:H. As in the case of a-Si:H, V_{oc} has a strong dependence on E_g(μc-Si:H) only when E_g is much smaller than the mobility gap of the intrinsic layer. Good agreement between simulated and measured values is obtained for E_g(μc-Si:H) equal to 1.59 eV. This is again consistent with the IPE results. It is interesting to note that for a wide range of discontinuity distributions, from zero to maximum offset at either the conduction or the valence band edge, both V_{oc} and FF are remarkably insensitive. This indicates that these parameters are governed more by the bulk properties.

The simulation of quantum efficiency of a-SiGe:H cells is less successful in explaining the experimental results. For all five cases listed in Table 16, the simulated Q ratio, i.e., the loss of carrier collection, is much lower than the measured value (see Table 17). Further simulation studies using different bulk and interface parameters will be necessary to understand this discrepancy.

Table 16. Simulated and Measured a-SiGe:H Alloy Cell Characteristics. A value of 1.63 eV is used for the mobility gap of a-SiGe:H in the simulation.

E_g(μc-Si:H) (eV)	$\Delta E_c/\Delta E_v$ (meV)	V_{oc} (V)	FF	Case #
1.90	-170/-100	0.75	0.61	5
1.59	-180/220	0.74	0.57	6
1.59	-90/130	0.74	0.58	7
1.59	0/40	0.74	0.60	8
1.10	-80/610	0.49	0.53	9
Measured		0.74	0.59	

Table 17. Ratio of Q(-3 V) to Q(0 V) of a-SiGe:H Alloy Cells.

E_g(μc-Si:H) (eV)	$\Delta E_c/\Delta E_v$ (meV)	λ(nm)	[Q(-3 V)/Q(0 V) - 1]×100 (%) 400	500	600	700	800	Case #
1.90	-170/-100		3.2	0.9	1.0	2.6	2.7	5
1.59	-180/220		1.5	0.6	1.1	3.2	2.6	6
1.59	-90/130		1.3	0.5	0.9	2.7	2.8	7
1.59	0/40		1.4	0.8	1.1	2.8	2.9	8
1.10	-80/610		1.4	0.7	2.1	5.5	5.7	9
Measured			13.4	7.2	5.1	6.9	10.8	

Conclusions

In conclusion, we have used IPE measurements to determine the electrical bandgap of microcrystalline *p* layers used in a-Si:H alloy solar cells, and the band edge discontinuities at the conduction and valence bands between μc-Si:H and a-Si:H alloy. The bandgap of μc-Si is found to be around 1.6 eV, and the discontinuities at the conduction and the valence band edges are -0.02 and 0.26 eV, respectively. Use of these parameters in the numerical simulation of single-junction a-Si:H and a-SiGe:H alloy solar cells is found to predict solar cell performance under global AM1.5 illumination. However, further understanding is needed to explain the loss of carrier collection in a-SiGe:H alloy cells.

Section 6

Analysis of Fill Factor Losses in a-Si:H and a-SiGe:H Alloy Solar Cells

Introduction

The multijunction multi-bandgap approach has proved to be successful for obtaining high efficiency solar cells and modules (Yang et al. 1988, Guha et al. 1994, Yang et al. 1994). An initial efficiency of 11.8% and stabilized efficiency of 10.2% have been reported on approximately one square foot aperture area modules (Guha et al. 1994, Yang et al. 1994). The derating factor in efficiency for increasing the cell area from 0.25 cm^2 active area to the module aperture area is small. Any further improvement in the module efficiency can be brought about only by first increasing the small area cell efficiency. In recent times, several techniques have been used to improve the component cell efficiency and reduce losses in the multijunction structure (Banerjee et al. 1994-1, Banerjee et al. 1994-2, Banerjee 1995). This section presents a new way to analyze losses in the *i* layer of single-junction a-Si:H and a-SiGe:H alloy *p i n* cells. Losses at the *p/i* interface and the bulk of the *i* layer have been investigated. The deleterious effect of substrate texture on cell performance has been explored.

There have been some studies carried out on especially the *p/i* junction loss. It was experimentally demonstrated (Arya et al. 1986, Schropp et al. 1993, Xi et al. 1994) that the open-circuit voltage, V_{oc}, the fill factor, FF, and the stability could be increased by interposing a thin interfacial graded layer and/or insulator layer between the *p* and the *i* layers of a *p i n* cell in which amorphous silicon-carbon (a-SiC) alloy was used as the p layer. Different explanations have been given for the carrier recombination losses occurring at the *p/i* interface and the beneficial role of the *p/i* interfacial layer. Boron contamination of the *i* layer from the underlying *p* layer, bond distortion and lattice mismatch at the *p/i* interface due to bandgap discontinuity, and back diffusion of electrons generated near the *p/i* interface are some such explanations. The wide bandgap buffer layer has been said to alleviate the boron diffusion and/or reduce back diffusion of electrons by separating the carrier generation area from the geometric interface as well as provide an electric field. Some modelling studies (Fantoni et al. 1994) of the role of thin defective buffer layers at both the *p/i* and *n/i* interfaces of *p i n* cells have been done.

All the work done to date on *p/i* and *n/i* junction losses has been carried out on cells made in the superstrate structure (glass/transparent conducting oxide/*p/i/n*/metal) in which the light is incident through the glass. In this configuration, the conventional *p* layer is either microcrystalline or amorphous SiC alloy. The inherent disadvantage is that the *p* layer is subjected to thermal stresses during the subsequent deposition of the overlying *i* and *n* layers which are normally done at higher temperatures. The microcrystalline *p* layer is especially susceptible to degradation during high temperature processing. Further, interdiffusion between the *p* and *i* layers elements is very likely. Use of C in the *p* layers makes the *p/i* junction even more complex. Thus, the superstrate structure is difficult to analyze.

In this study, we have used the substrate configuration (ss/*n/i/p*/transparent conducting oxide) to study the losses. Basically, the technique consists of the comparison of the ratio of quantum efficiency, Q, measured under reverse bias, Q(-), and zero bias, Q(0), with the fill factor measured under blue, FF_b, and red, FF_r, light illumination. A technique to reduce the losses is also described. The results provide important feedback for designing a better device.

Experimental

Both a-Si:H and a-SiGe:H alloy cells were deposited in the substrate configuration on stainless steel substrates, (ss) without any back reflector and textured Ag/ZnO back reflectors (BR) by conventional glow discharge technique. Three different types of cells were made: (1) a-Si:H alloy with *i* layer thickness 250-270 nm, (2) intermediate bandgap a-SiGe:H alloy with *i* layer thickness 150-170 nm and (3) narrow bandgap a-SiGe:H alloy with *i* layer thickness 140-160 nm. The Q curves of the cells were measured as a function of wavelength. The current-voltage, IV, characteristics were measured under AM 1.5 illumination, and under blue and red light illumination using narrow band-pass filters centered at 390 and 670 nm, respectively.

Results and Discussion

The Q loss curves, Q_L, defined as Q(-)/Q(0), as a function of wavelength of the a-Si:H alloy cells are shown in Fig. 5. The value of Q_L qualitatively denotes the carrier collection loss in the *i* layer: higher values represent higher losses. Samples 1Sa and 1Bb are cells made on ss and BR, respectively; S denotes stainless steel and B back reflector. The collection losses increase at both low and high wavelengths displaying a minimum at ~500 nm. The BR sample displays a higher loss across the entire wavelength range compared to the ss sample. Samples 1Bc and 1Sd (see Fig. 5) are similar to samples 1Bb and 1Sa, respectively, except that two thin interfacial *i* layers are interposed between the *p/i* and *n/i* junctions. Comparison of the samples 1Bc with 1Bb and 1Sd with 1Sa shows that the reduction in the collection loss is across the entire wavelength spectrum. The fractional gain is higher for the BR sample. The ss sample shows a gain mainly in the low wavelength regime. In order to separate the effects of the two interfacial layers, sample 1Be was made on BR which is equivalent to sample 1Bb except that it has only a *p/i* interfacial layer. Figure 6 compares the losses of the two samples 1Bb and 1Be. It is clear that the gain in this case is primarily in the blue part. The small gain in the red is probably a run to run variation.

The IV characteristics of the samples shown in Figs. 5 and 6 are summarized in Table 18. The values of only the open-circuit voltage, V_{oc}, measured under AM 1.5 illumination and FF_b and FF_r are shown. Comparison of the results of samples 1Sa and 1Bb show that the substrate texture has a deleterious effect on primarily the FF_b and to a certain extent on the V_{oc} and FF_r. The values of FF_b and FF_r for the samples 1Sa and 1Bb are 0.767 and 0.701, respectively, and 0.696 and 0.683, respectively. The samples 1Bc (with the double interfacial layers) shows an improvement in the values of FF_b and FF_r to 0.732 and 0.719, respectively, and V_{oc} to 0.977 V. Sample 1Sd also exhibits similar gains in FF_b and FF_r to 0.788 and 0.725, respectively, and V_{oc} to 0.995 V. Sample 1Be (with only the *p/i* interfacial layer) shows a gain primarily in FF_b to 0.718; FF_r is similar, 0.687, and V_{oc} increases to 0.964 V.

Other a-Si:H alloy cells with different thicknesses of *p/i* interfacial layers have been fabricated on back reflectors. The value of FF_b initially increases and then decreases with increasing thickness of the interfacial layer. The value of the FF_r is independent of the thickness of the layer.

An analysis of the above data elucidates the strong correlation between the Q_L data in Figs. 5 and 6 and the IV results shown in Table 18. High values of FF_b are associated with low values of Q_L in the lower wavelength regime and vice versa. FF_r and Q_L in the higher wavelength regime enjoy a similar inter-relationship. The increase in Q_L with decreasing wavelength at low wavelengths is attributed to back diffusion of electrons from the front surface of the cell where blue light is strongly absorbed. The increase in Q_L at wavelengths $\geq$500 nm is more difficult to interpret since the light is absorbed reasonably uniformly across the thickness of the *i*-layer. The substrate texture has a deleterious effect on the cell performance: FF_b decreases and Q_L in the entire wavelength regime increases. The lower FF_b and higher Q_L in the blue part are attributed to enhanced back diffusion of electrons near the *p/i* interface due to the

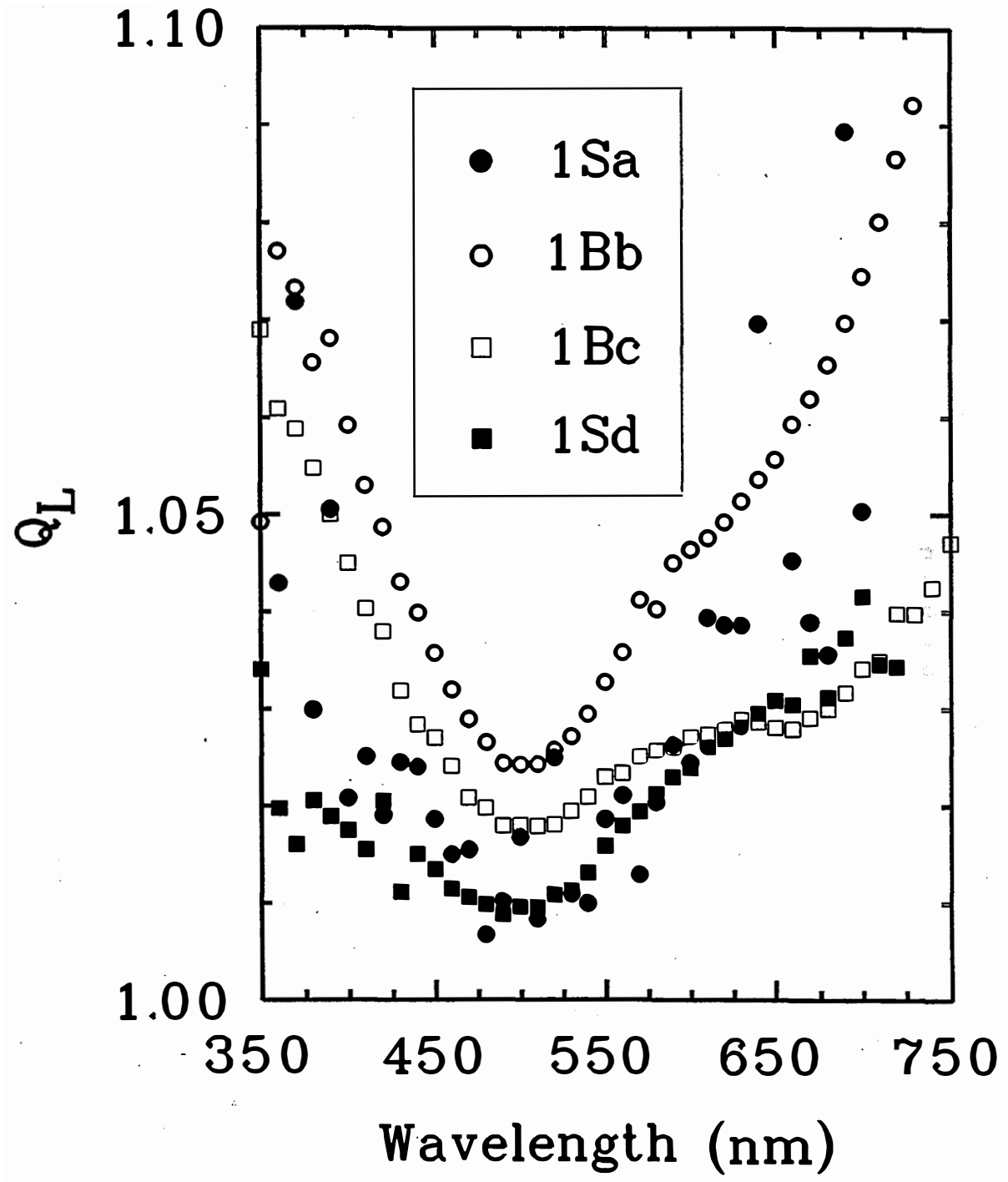

Figure 5. **Q_L curves of the a-Si:H alloy cells.**
Refer to Table 18 for sample description.

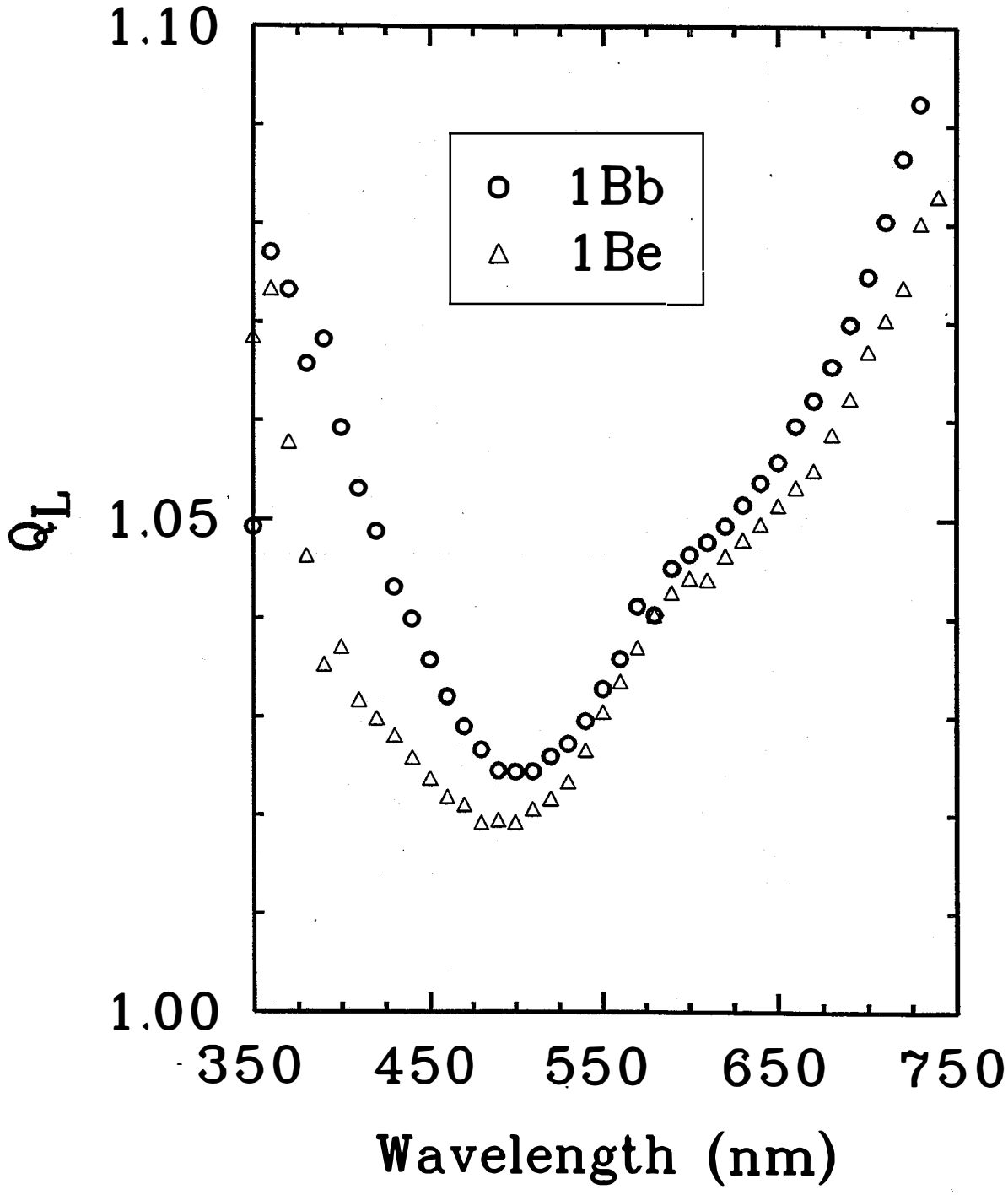

Figure 6. **Q_L curves of the a-Si:H alloy cells with and without interfacial layer.**

enhanced effective *p/i* junction area. The higher Q_L at wavelengths ≥500 nm is attributed to poorer carrier collection in the *i* layer. The role of the interfacial layers is to introduce wide bandgap layers at the junctions. The *p/i* interfacial layer leads to higher FF_b and lower Q_L in the blue part and this is attributed to reduced back diffusion effects in view of less carrier generation. The effect of the *n/i* interfacial layer is the enhancement of FF_r and reduction in Q_L over the entire wavelength range. The role of the *n/i* layer is more difficult to interpret but it appears that it improves the carrier collection in the bulk of the *i* layer.

Figure 7 shows the Q_L curves of the intermediate bandgap a-SiGe:H alloy cells. Sample 2Sa and 2Bb are equivalent devices on ss and BR substrates, respectively. Sample 2Zc is a cell on a textured ZnO film deposited on ss substrate: this substrate provides a poorly reflecting textured surface. Sample 2Bd is similar to 2Bb except that it has two thin interfacial *i* layers at the *p/i* and *n/i* junctions. The results are qualitatively similar to the a-Si:H alloy cells shown in Figs. 5 and 6. The losses are higher at the low and high wavelengths. Comparison of samples 2Bb and 2Zc with 2Sa shows that the substrate texture has a deleterious impact on Q_L over the entire spectrum. The Q_L for samples 2Bb and 2Zc are almost similar: sample 2Zc exhibits slightly lower loss at ~670 nm (wavelength at which FF_r is measured). Incorporation of the interfacial layers has an alleviating effect on Q_L: sample 2Bd exhibits Q_L as low as 2Sa except in the blue where it is slightly higher.

The IV characteristics of the cells shown in Fig. 7 are summarized in Table 19. The qualitative results are again similar to the a-Si:H alloy cells tabulated in Table 18. The ss sample 2Sa has V_{oc}, FF_b, and FF_r values of 0.793 V, 0.714, and 0.697, respectively. The BR sample 2Bb exhibits a deterioration in the values of FF_b and FF_r to 0.645 and 0.666, respectively. The value of V_{oc} is similar. The ZnO sample has similar values of V_{oc} and FF_b of 0.785 and 0.635, respectively, and slightly higher value of FF_r, 0.684, compared to sample 2Bb. The sample 2Bd with the interfacial layers leads to a partial recovery of FF_b and FF_r to 0.685 and 0.690, respectively. The V_{oc} is higher, 0.818 V.

The correlation and explanation of the inter-relationship between FF_b and Q_L in the blue part and between FF_r and Q_L in the higher wavelength regime is similar to the one offered earlier for the a-Si:H cells. The texture of the substrate due to the ZnO film is primarily responsible for the degradation of the cell characteristics as shown by the similar results of samples 2Bb and 2Zc. The Ag film has a small effect as seen by the comparison of the FF_r.

The Q_L curves and the summary of the IV characteristics of the narrow bandgap a-SiGe:H alloy cells are shown in Fig. 8 and Table 19, respectively. The Q_L curves are similar to the ones presented earlier. It may be noted that the reverse bias applied for the Q(-) measurements for all the data presented in this paper is the same. This leads to the underestimation of the value of Q_L for the poorer quality a-SiGe:H alloy samples but the results are still valid. The BR sample 3Bb has lower values of FF_b, 0.648, and FF_r, 0.656, compared to the corresponding values of 0.698 and 0.687, respectively, for the ss sample 3Sa. The effect of the interfacial layers is less: the FF_r does not change and the FF_b increases marginally to 0.661. This is attributed to the poorer quality of the films limiting the device performance. For both series 2 and 3 samples, FF_b and FF_r for the interfacial layer cases are lower than the corresponding ss values.

Conclusion

In conclusion, the Q_L measurement technique provides a strong correlation with the cell performance under colored light. Higher values of Q_L in the low wavelength regime is associated with back diffusion losses at the *p/i* interface and affects FF* '(*^U*^U29^\er Q_L values in the high wavelength regime is mainly due to bulk losses in the *i* layer and is accompanied by inferior FF_r. The technique has been used to understand some of the causes for the poorer cell results on textured substrates. The analysis has helped in finding ways to improve the device performance on textured back reflectors.

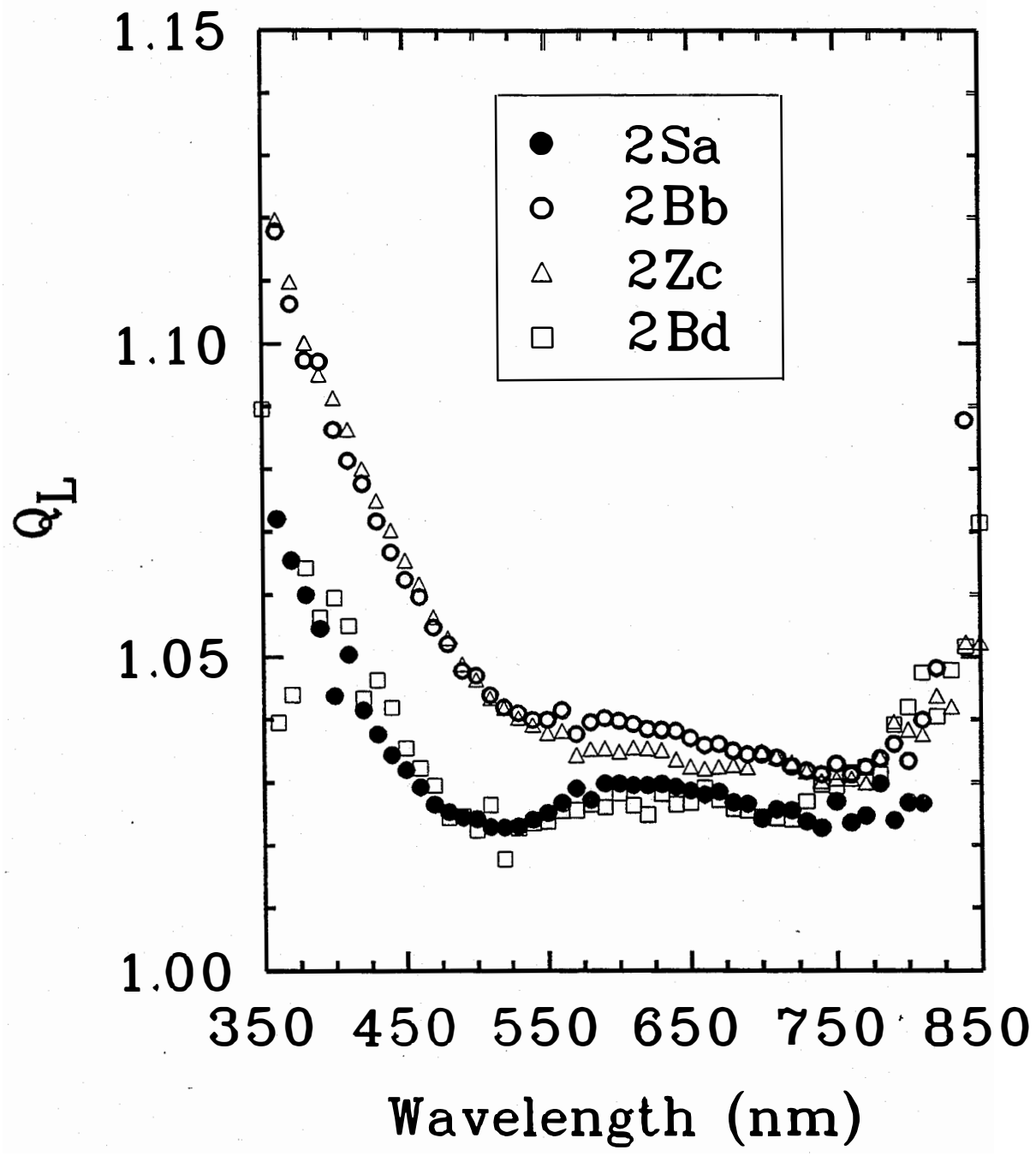

Figure 7. **Q_L curves of intermediate bandgap a-SiGe:H alloy cells.** Refer to Table 19 for sample description.

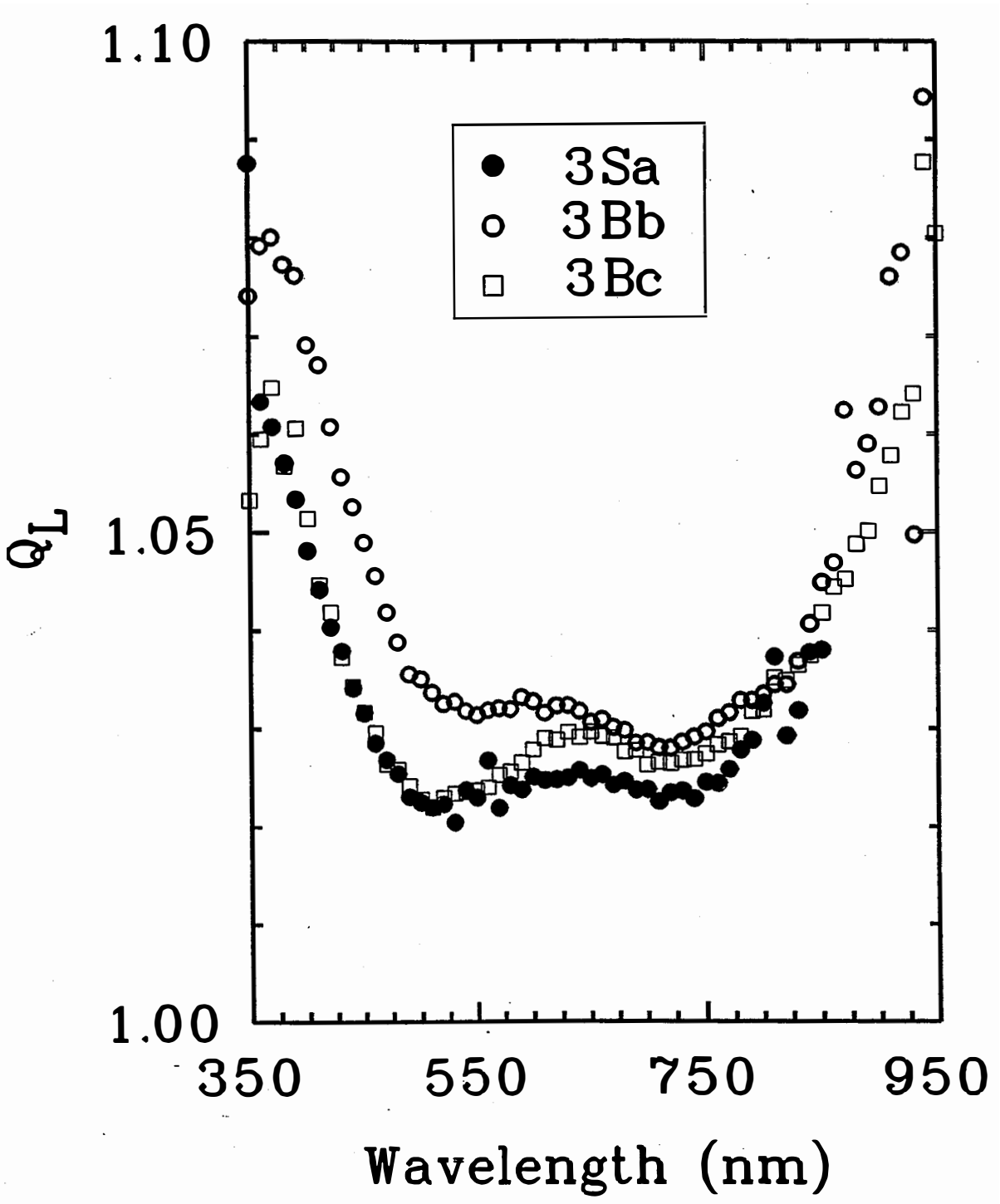

Figure 8. **Q_L curves of narrow bandgap a-SiGe:H alloy cells.** Refer to Table 19 for sample description.

Table 18. V_{oc}, FF_b, and FF_r of the a-Si:H Alloy Cells.

Sample	Sub.	Description	V_{oc} (Volts)	FF_b	FF_r
1Sa	ss	standard	0.975	0.767	0.701
1Bb	BR	standard	0.949	0.696	0.683
1Bc	BR	p/i, n/i interface layers	0.977	0.732	0.719
1Sd	ss	p/i, n/i interface layers	0.995	0.788	0.725
1Be	BR	p/i interface layer	0.964	0.718	0.687

Table 19. V_{oc}, FF_b, and FF_r of the Intermediate (I) and Narrow (N) Bandgap a-SiGe:H Alloy Cells.

Sample	Bandgap	Description	Sub.	V_{oc} (Volts)	FF_b	FF_r
2Sa	I	standard	ss	0.793	0.714	0.697
2Bb	I	standard	BR	0.787	0.645	0.666
2Zc	I	standard	ZnO	0.785	0.635	0.684
2Bd	I	*p/i, n/i* interface layers	BR	0.818	0.685	0.690
3Sa	N	standard	ss	0.687	0.698	0.687
3Bb	N	standard	BR	0.688	0.648	0.656
3Bc	N	*p/i, n/i* interface layers	BR	0.719	0.661	0.655

Section 7

Analysis of Carrier Collection Losses in a-Si:H and a-SiGe:H Solar Cells

Introduction

In recent years, the gap between the highest small area cell efficiency (Yang et al. 1988) and the highest module efficiency (Guha et al. 1994) has been narrowed considerably. In order to make any significant improvement in the module efficiency, it is necessary to improve the small area cell efficiency first. In our continuing effort towards achieving this objective, we have explored (Banerjee et al. 1994-1, Banerjee et al. 1994-2, Banerjee 1995) different loss mechanisms occurring in the cells. This paper presents experimental evidence of losses existing in the bulk *i* layer and near the *p/i* interface of both a-Si:H and a-SiGe:H alloy *p i n* cells.

There have been some studies carried out on the *p/i* junction loss. It was experimentally demonstrated (Arya et al. 1986, Schropp et al. 1993, Xi et al. 1994) that the open-circuit voltage, V_{oc}, the fill factor, FF, and the stability could be increased by interposing a thin interfacial graded layer and/or insulator layer between the *p* and the *i* layers of a *p i n* cell in which a-SiC was used as the *p* layer. Some modelling studies (Fantoni et al. 1994) of the role of thin defective buffer layers at both the *p/i* and *n/i* interfaces of *p i n* cells have been done. As discussed in Section 6, all work done to date on *p/i* and *n/i* junction losses have been carried out on cells made in the superstrate structure (glass/TCO/*p*/*i*/*n*/metal) in which the light is incident through the glass. In this configuration, the conventional *p* layer is either microcrystalline or amorphous SiC alloy. The inherent disadvantage is that the *p* layer is subjected to thermal stresses during the subsequent deposition of the overlying *i* and *n* layers which are normally done at higher temperatures. The microcrystalline *p* layer is especially susceptible to degradation during high temperature processing. Further, interdiffusion between the *p* and *i* layers elements is very likely. Use of C in the *p* layers makes the *p/i* junction even more complex. Thus, the superstrate structure is more difficult to analyze.

In this study, we have used the substrate configuration (metal/*n*/*i*/*p*/TCO), where the *p* layer is the last glow-deposited layer, to study the losses using reverse biased quantum efficiency, Q, and FF under blue and red light measurements. The paper describes the collection loss near the *p/i* junction and the bulk of the *i* layer and interface passivation techniques to improve the cell performance. The results have uncovered possible inhomogeneities in the direction of a-Si:H alloy film growth which are dependent on the deposition conditions.

Experimental

Both a-Si:H and a-SiGe:H alloy cells were deposited on stainless steel substrates (without any back reflector) by conventional glow discharge technique. The loss in the *i* layer was studied as a function of four variables: (1) optical bandgap, (2) thickness, (3) material quality, and (4) plasma treatment of the *n* surface. Two optical gap materials a-Si:H (~1.77 eV) and a-SiGe:H (~1.45 eV) alloys were used. Three different material qualities were investigated: a-Si:H, a-SiGe:H, and light-degraded a-SiGe:H alloy cells. The thicknesses of the *i* layers of the a-Si:H alloy cells were 120 nm for samples 1 and 2 and 250 nm for sample 3 and those of the a-SiGe:H alloy cells 4, 5, and 6 were 140, 280, and 560 nm, respectively. Sample 2 was subjected to a plasma treatment after the *n* layer deposition. The values of FF under blue and red light illumination, FF_b and FF_r, respectively, were measured using narrow-band-pass filters

centered at 390 nm and 670 nm, respectively. The values of Q versus wavelength were obtained for both zero bias, Q(0), and negative bias, Q(-) and the Q_{loss}, defined as the ratio of Q(-) to Q(0) was plotted. The values of the negative bias for the 120 nm a-Si:H, 250 nm a-Si:H, and the a-SiGe:H alloy cells were -1V, -2V, and -3V, respectively. The a-SiGe:H alloy cells 5 and 6 were light soaked for over 1000 hours and then remeasured.

Results and Discussion

The results of the Q_{loss} versus wavelength measurements for the a-Si:H alloy cells are shown in Fig. 9. All the samples exhibit a similar behavior: the Q_{loss} is higher at the low and high wavelength regimes with a minimum at intermediate wavelengths. The blue light is strongly absorbed near the front surface of the cell. The higher loss at these wavelengths has been shown (Banerjee et al. 1995) to be due to the back diffusion of the relatively high concentration of electrons from near the *p/i* interface. Intermediate wavelength ~500 nm light is also absorbed, but less strongly, near the front surface of the cell and results in a lower loss since back diffusion effects are less important at this wavelength. The excess loss at higher wavelengths >470 nm for samples 1 and 3 is difficult to interpret since the red light is uniformly absorbed in the *i* layer. In general, the red Q_{loss} can be attributed to losses across the entire thickness (bulk) of the sample.

The values of FF_b and FF_r of the a-Si:H alloy cells are summarized in Table 20. FF_b, measured using 390 nm light, is a measure of electron transport from the front surface of the cell where the monochromatic light is strongly absorbed to the back. Similarly, FF_r is a measure of the hole transport property in the bulk of the *i* layer. As reported (Banerjee et al. 1995), the values of FF_b and FF_r have a correlation with the Q_{loss} values at 390 nm and 670 nm, respectively. High values of FF_b and FF_r are associated with low values of Q_{loss} at 390 nm and 670 nm, respectively, and vice versa.

Table 20. Thickness, FF_b, and FF_r of a-Si:H and a-SiGe:H Cells.

Sample	*i* layer	*i* thickness (nm)	FF_b		FF_r	
			Initial	Degraded	Initial	Degraded
1	a-Si:H	120	0.77		0.69	
2	a-Si:H	120	0.78		0.77	
3	a-Si:H	250	0.79		0.72	
4	a-SiGe:H	150	0.69		0.68	
5	a-SiGe:H	280	0.67	0.58	0.69	0.56
6	a-SiGe:H	560	0.65	0.46	0.59	0.48

Sample 2 exhibits anomalous low Q_{loss} at wavelengths >470 nm (see Fig. 9) and high FF_r (see Table 20) compared to sample 1. The FF_r of samples 1 and 2 are 0.69 and 0.77, respectively, even though the FF_b for both samples are similar, 0.77 - 0.78. This result implies that the carrier collection in the bulk of the *i* layer is superior for sample 2. This is a surprising result since the only difference between the two samples is that sample 2 has been subjected to an additional plasma treatment after the *n* layer. There are three possible roles of the plasma treatment: (1) it reduces/eliminates any potential barrier at the *n/i* interface, (2) it produces a thin layer with very different material properties which readjusts the electric field distribution in the *i* layer resulting in superior current collection, and (3) it creates a surface which

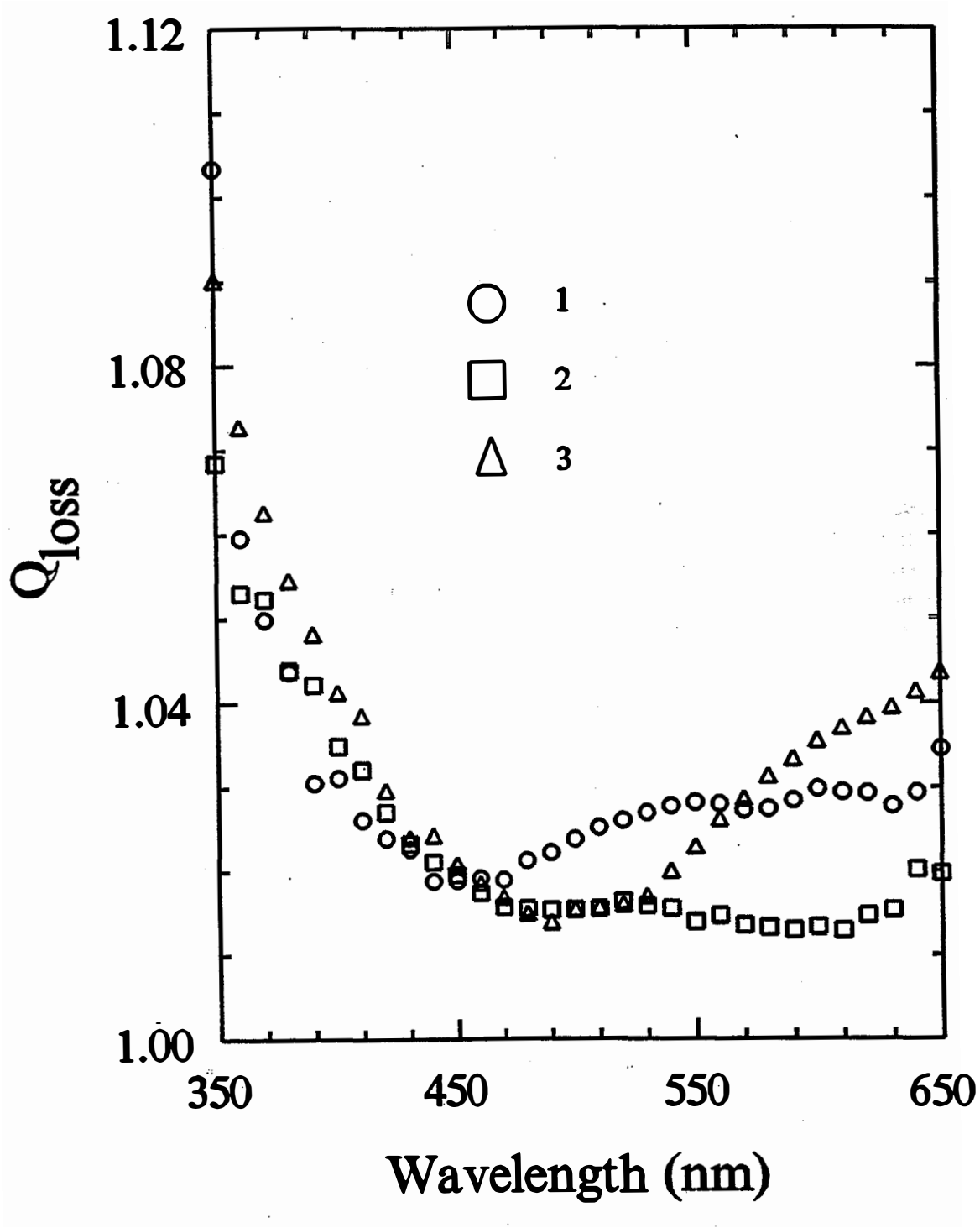

Figure 9. Q_{loss} **versus wavelength of the a-Si:H alloy cells.** Refer to Table 20 for sample description.

is congenial for the growth of low defect density *i* layer material. The first phenomenon is unlikely since the respective band edges on both sides of the amorphous *n/i* junction are expected to line up. In such a scenario it is not possible to have any significant barrier at the junction. In order to test the second hypothesis, we have simulated the values of Q_{loss} and fill factor of cells with and without a thin interfacial layer at the *n/i* junction using the AMPS model developed by Penn State University (Arch et al. 1991). In the model, the *i* layer was assigned a certain defect density and the defect density of the thin *n/i* interfacial layer was varied over one order of magnitude both lower and higher than the designated value for the *i* layer. The parameters were selected such that the model simulated the results of sample 1 fairly well. However, it failed to match the experimental values of Q_{loss}, FF_b, and FF_r of sample 2. In fact, the modelling showed that the effect of the interface layer on the device characteristics was small despite the large changes (two orders of magnitude) in the properties of the interfacial layer. This result eliminates the second hypothesis. Thus, the only viable explanation of the low Q_{loss} in the red and high FF_r of sample 2 is the improvement of the material quality in the bulk of the *i* layer. This result has an important implication: the quality of the *i* layer and thereby the film growth mechanism is dependent on the surface properties of the substrate and predeposition conditions. The *i* layer deposited directly on an *n* layer possesses a higher concentration of defect density than on a "passivated" surface. On a textured surface the losses have been reported (Banerjee et al. 1995) to be even higher.

It may be expected that the properties of the *i* layer become independent of the substrate material beyond a certain thickness which in turn would imply an inhomogeneity in the material properties in the direction of film growth. In fact, this is borne out by the shape of the Q_{loss} curve of the thicker sample 3. The loss is as low as that of sample 2 at the wavelength ~500 nm (see Fig. 9), even though the sample is thicker and no "passivation" was done after the *n* layer. It is not clear why the value of FF_r, 0.72, is higher than that of sample 1. Tentatively, based on the earlier hypothesis that the *i* layer initially grows on an untreated *n* layer with higher defect density, the thicker sample is expected to absorb a certain portion of the light in the better quality top half of the cell which would then lead to a superior "average" value of FF_r results. The Q_{loss} exhibits steeper "wings" in the low and high wavelength regimes: the losses rise faster in these two regions. The increase in losses in the wavelength ranges 400 - 500 nm and 500 - 650 nm are attributed to the extra thickness (compared to samples 1 and 2) the photogenerated electrons and holes, respectively, have to travel before they are collected.

The above results imply that at least in the device configuration the *i* layer suffers from inhomogeneities in the transverse direction: the defect density initially decreases with increasing thickness before reaching a saturation value after a decay length of a few tens of nanometers. Curtins and Favre (1989) have reported a similar phenomenon in very high frequency glow discharge intrinsic a-Si:H alloy films deposited at a high rate of 1 - 2 nm/s. Their conclusion was derived from trying to model the deep and shallow defect density obtained by photothermal deflection spectroscopy for thick films. They reported a much higher decay length of ~1 μm. In order to reconcile with both the results it may be speculated that the material quality during the initial phase of growth depends on a host of conditions such as nature of the plasma reactor, deposition rate and frequency, plasma treatment, substrate preparation, etc. The scope of the present work is to suggest the existence of the complex interrelationship amongst the parameters listed above. Detailed work is necessary for a better understanding of the phenomena.

Figure 10 displays the Q_{loss} for the a-SiGe:H alloy cells. The initial characteristics (shown in open symbols) are qualitatively similar to the a-Si:H alloy results. The differences are discussed. The front surface back diffusion losses extend to higher wavelengths: comparison of the thinnest samples (1, 2, and 4) in Figs. 9 and 10 shows that for the a-Si:H alloy cells, the losses extend to 450 - 480 nm whereas for the a-SiGe:H alloy cells, the losses extend beyond to 500 - 550 nm. This is attributed to the higher absorption coefficient of the a-SiGe:H alloy films. Further, the absolute value of the Q_{loss} over the entire spectrum is higher in view of the poorer quality of the a-SiGe:H alloy *i* layers. The thickness dependence

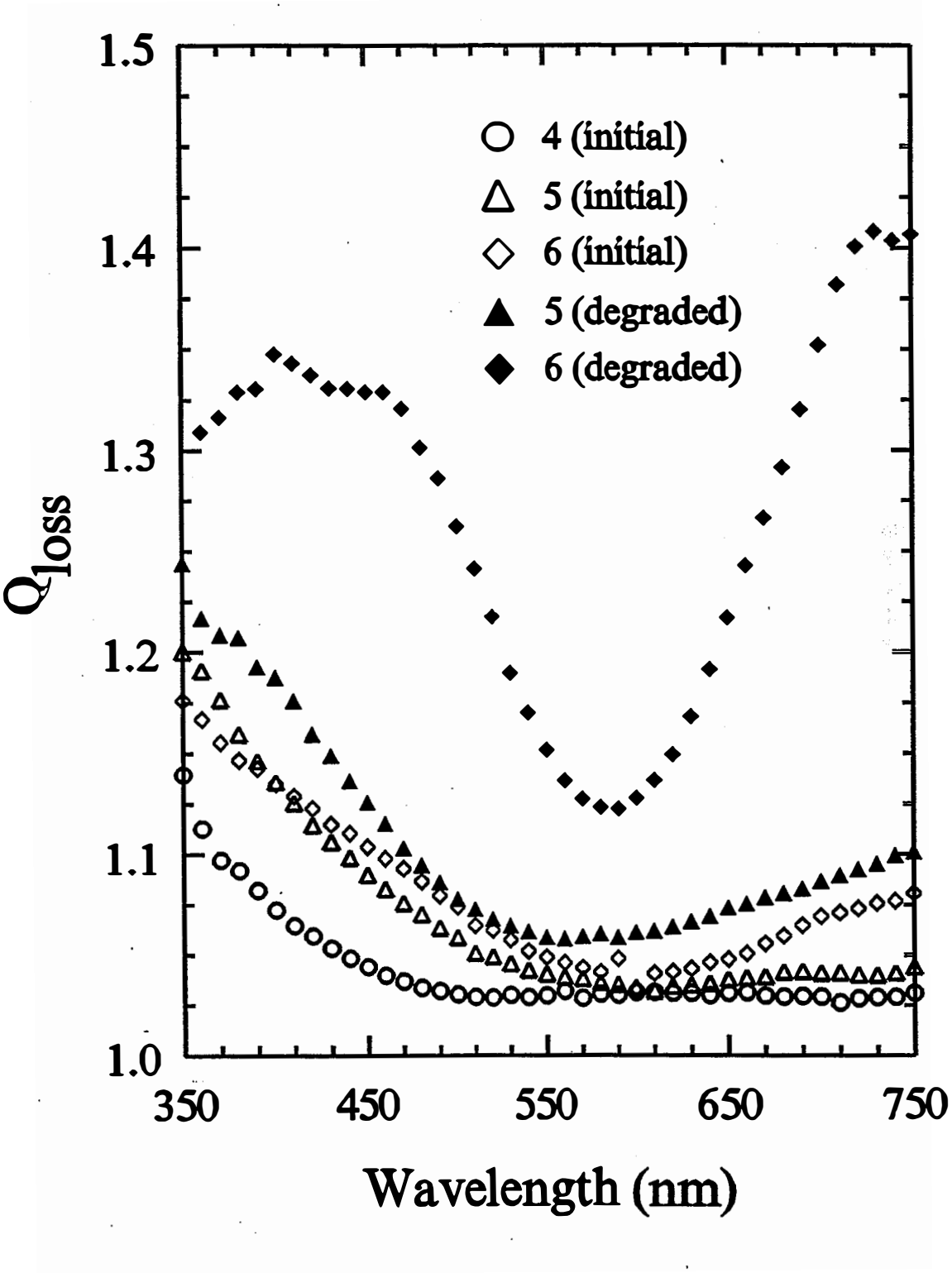

Figure 10. Q_{loss} versus wavelength of the a-SiGe:H alloy cells.
Refer to Table 20 for sample description.

and the corresponding explanation of the Q_{loss} in terms of the characteristic steeper "wings" at the lower and higher wavelengths are similar to the a-Si:H alloy case. The results of the light-degraded a-SiGe:H alloy samples 5 and 6 are shown in Fig. 10. Compared to the initial values, the degraded results expectedly exhibit greater losses. The losses in the "wings" regions increase faster: the effect in the thicker sample 6 is more pronounced. As explained earlier, the losses in the "wings" are attributed to the bulk where the photogenerated carriers have to travel over long distances before they can be collected. Light soaking adversely affects collection losses for both electrons and holes. The enhanced losses are attributed to the poorer transport properties of the carriers. The behavior of the degraded sample 6 in the wavelength range 350 - 400 nm is anomalous and further work needs to be done to understand it.

The colored FF results of the a-SiGe:H alloy cells are summarized in Table 20. The initial results show that the value of FF_b deteriorates progressively from 0.69 to 0.65 as the thickness of the *i* layer is increased from sample 4 to sample 6. The Q_{loss} trend (see Fig. 10) is similar. The values of FF_r for samples 4 an 5 are similar ~0.68-0.69; for the thickest sample 6 it is only 0.59. The Q_{loss} curves at 670 nm reflect a similar trend. The lower values of FF_b and FF_r of the light soaked samples also have a good correlation with the corresponding Q_{loss} behavior.

Conclusion

In conclusion, carrier collection losses in the front surface and the bulk of the *i* layer of a-Si:H and a-SiGe:H alloy cells have been identified using the Q_{loss} technique. The quality of the a-Si:H alloy film appears to be dependent on the nature of the surface on which it grows. There is some evidence of inhomogeneity in the material properties of the a-Si:H alloy film along the direction of film growth in the device configuration. The deposition conditions play an important role in determining the properties of the initial growth phase. The bulk loss increases with increasing *i* layer thickness as well as with decreasing material quality. Light soaking has a deleterious effect on both electron and hole transport. There is a strong correlation between the Q_{loss} and the values of the colored FF.

Section 8

Status of a-Si:H and a-SiGe:H Component Cells and Triple-Junction Performance

Introduction

To achieve high-efficiency triple-junction cells, several key issues need to be addressed. These include high quality (1) back reflectors, (2) component cells, (3) "tunnel" junctions, (4) transparent conducting oxide, and (5) cell matching. From the previous sections, it is obvious that substantial work has been carried out to improve the material quality and device structure. We shall report the status of the component cells and triple-junction devices here.

Status of Component Cells

We should first mention that for the design of the component cells, our goal is to obtain high efficiency triple-junction cells having a J_{sc} of about 8 mA/cm^2. This implies that each component cell should produce at least 8 mA/cm^2 in current density. Since the top and middle cells in a triple-junction solar cell stack do not receive much reflected light, we deposited the component cells onto bare stainless steel substrates without the Ag/ZnO back reflectors for evaluation.

For the top cell, we used an a-Si:H alloy without incorporation of carbon. By using hydrogen dilution to improve the quality of the *i* layer and incorporating a microcrystalline *p* layer to enhance the built-in potential, we have obtained an initial V_{oc} of 1.014 V, a FF of 0.78, and a J_{sc} of 8.65 mA/cm^2. The J-V characteristic is shown in Fig. 11. This is the best performance of a top cell reported in the literature. We should mention that one could obtain a higher V_{oc} if one uses a wider band gap *i* layer. In fact, we have made a wider bandgap top cell with larger hydrogen incorporation in the *i* layer and achieved a V_{oc} of 1.056 volts. However, the stability of the cell is poorer.

For the middle cell, we used a high hydrogen diluted gas mixture of Si_2H_6 and GeH_4 in the *i* layer. The J-V characteristic measured with AM1.5 through a 530 nm cut-on filter is shown in Fig. 12. One notes that J_{sc} is greater than 9 mA/cm^2, and both V_{oc} and FF show high values. The 530 nm filter was used to simulate the middle cell's insolation in a triple-junction structure. A 630 nm filter is used when evaluating a bottom component cell for the same reasons. The bottom cell incorporated an a-SiGe:H alloy *i* layer with high hydrogen dilution and was deposited onto a Ag/ZnO back reflector. The J-V characteristic measured with AM1.5 through a 630 nm cut-on filter is shown in Fig. 13. The initial power output of 4.43 mW/cm^2 is the highest reported to date. These results also reflect the improvement that has been made on the quality of the a-SiGe:H alloy. Table 21 summarizes the initial photovoltaic characteristics of the component cells obtained with high hydrogen dilution. It is anticipated that when the improved component cells are incorporated in a triple-junction structure with proper current matching, an initial cell efficiency exceeding 14% can be obtained. This would certainly lead to higher module efficiencies.

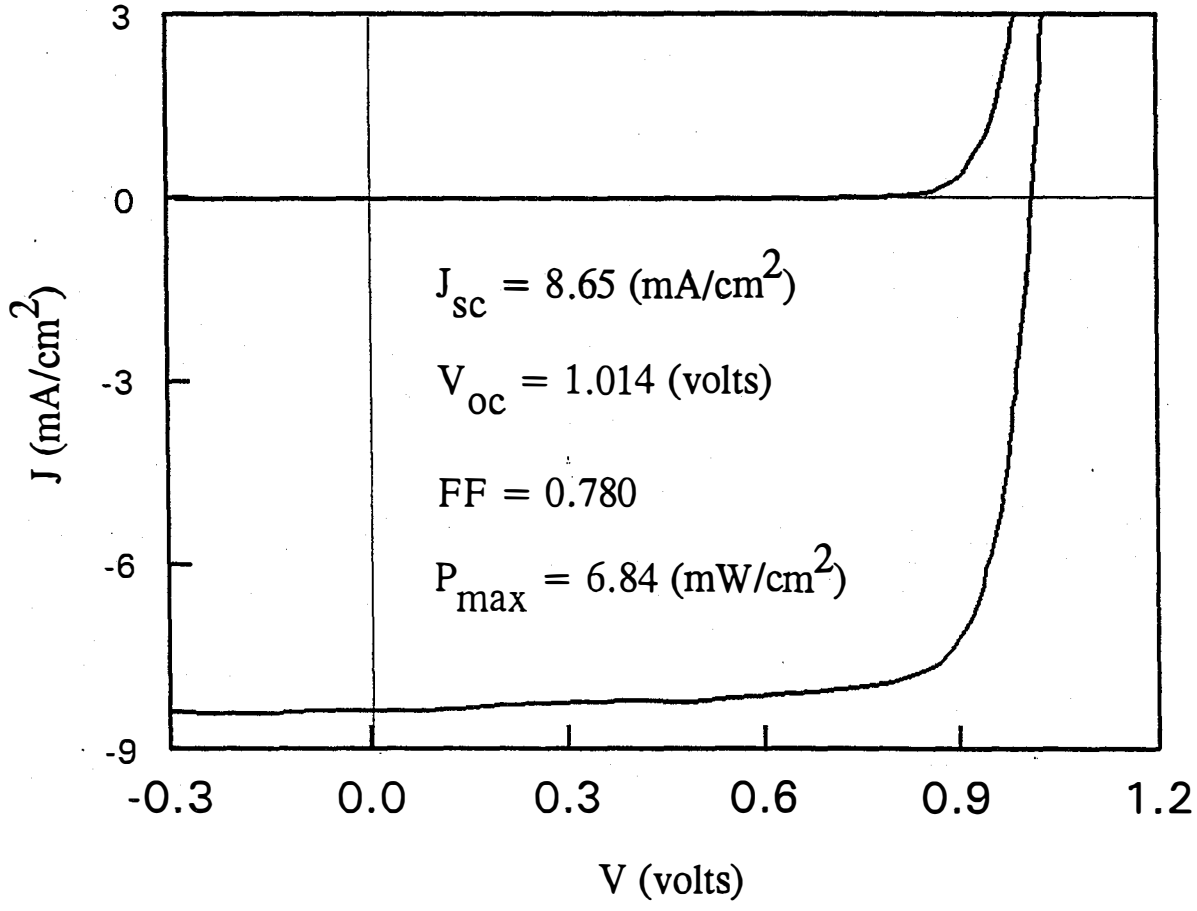

Figure 11. **Initial J-V characteristic of the top cell measured under AM1.5.**

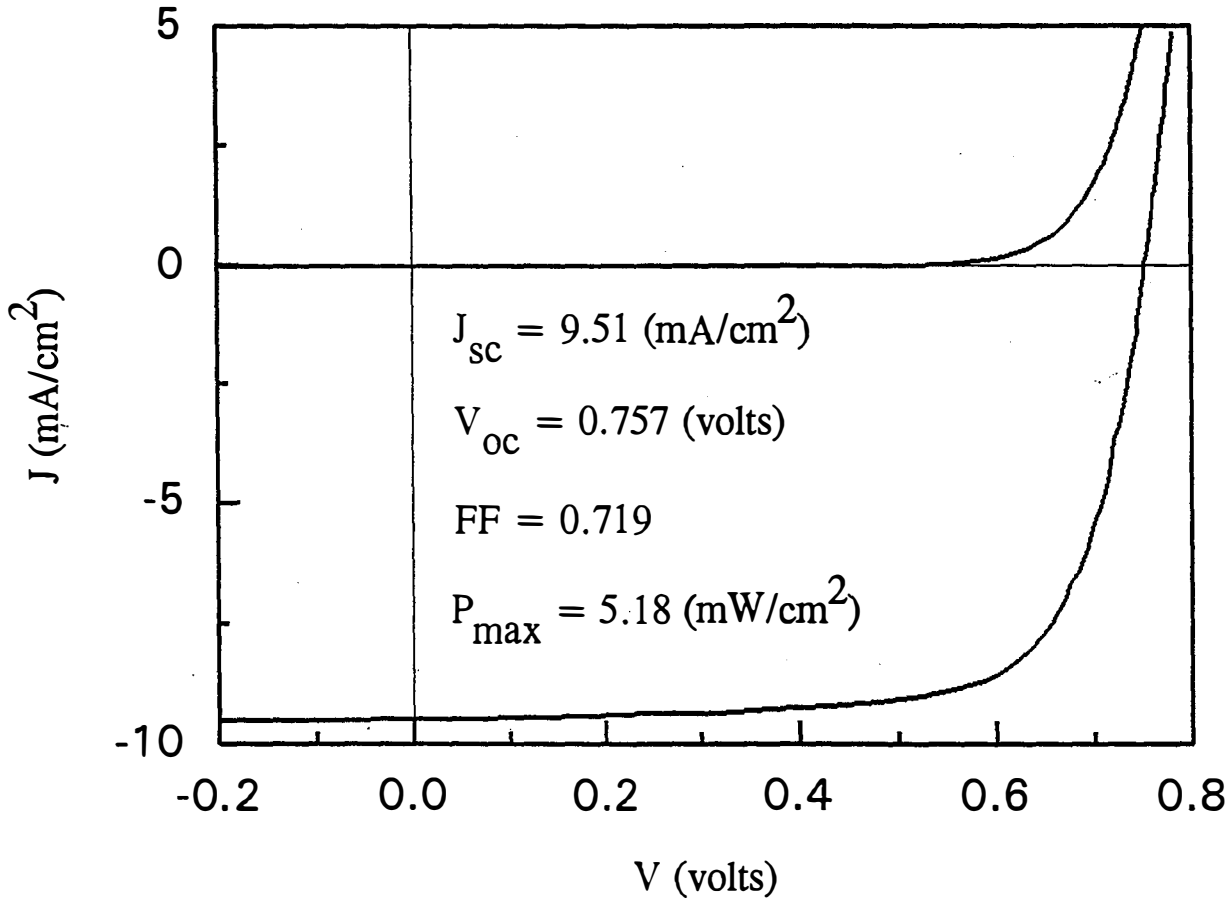

Figure 12. **Initial J-V characteristic of the middle cell measured under AM1.5 with a 530 nm cut-on filter.**

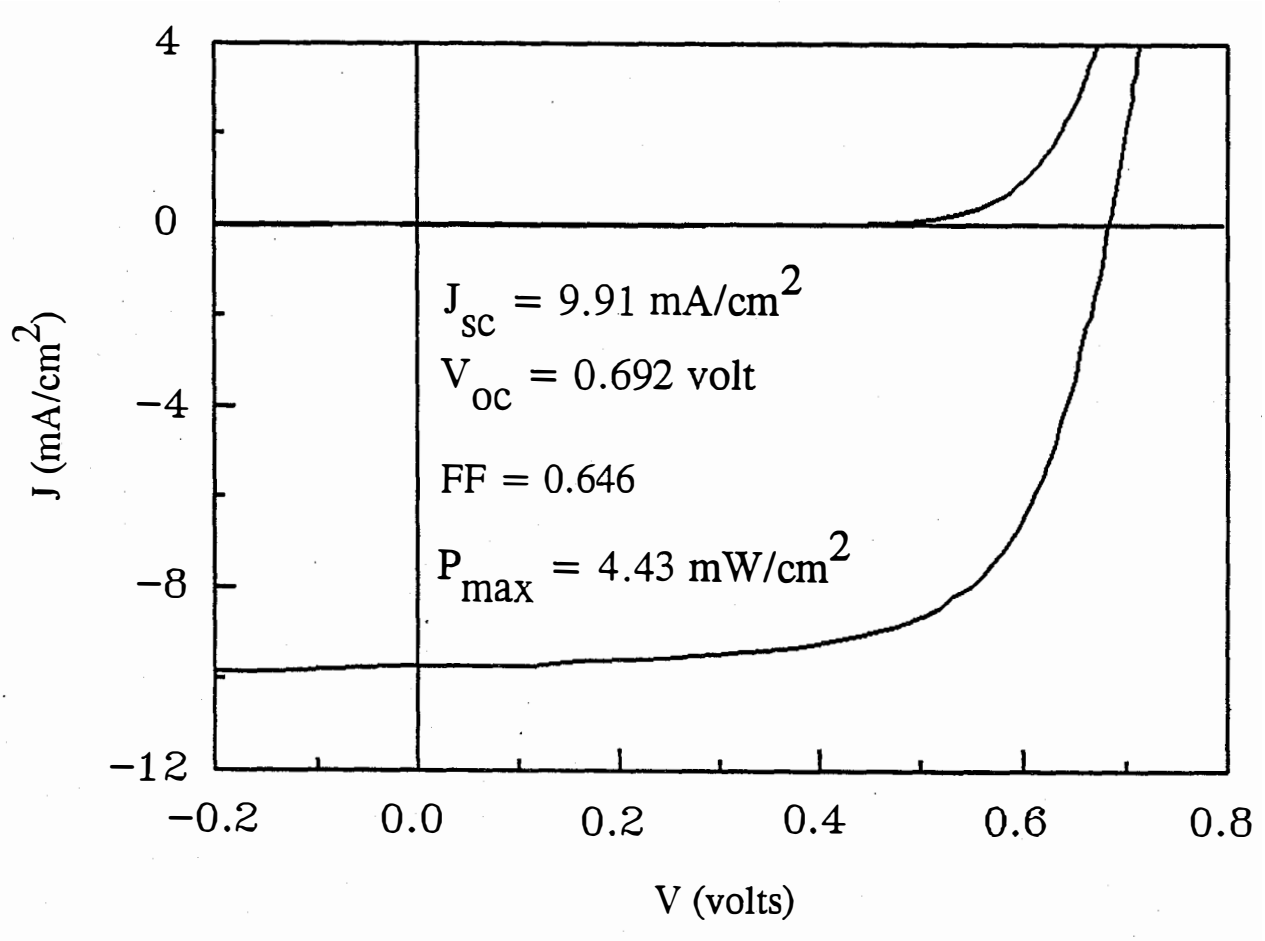

Figure 13. **Initial J-V characteristic of the bottom cell measured under AM1.5 with a 630 nm cut-on filter.**

Table 21. Best Initial J-V Characteristics of the Component Cells at United Solar.

Component Cell	J_{sc} (mA/cm^2)	V_{oc} (V)	FF	P_{max} (mW/cm^2)
Top*O	8.65	1.014	0.780	6.84
Middle*▲	9.51	0.757	0.719	5.18
Bottom†□	9.91	0.692	0.646	4.43

* deposited on bare stainless steel
† deposited on textured Ag/ZnO
O measured under AM 1.5
▲ measured under AM 1.5 with a λ>530 nm filter
□ measured under AM 1.5 with a λ>630 nm filter

Stability of Component Cells

To study the stability of the component cells, we used a metal-halide lamp with the intensity adjusted to one sun. Appropriate filters were used for the middle and bottom cells to simulate their operations in a triple-junction solar cell stack. We should also mention that the top and middle cells for the light soaking experiment were deposited on textured substrates overcoated with Cr, since they do not receive much reflected light in a triple structure. For J-V measurements, the top cell was measured with AM 1.5 light, while the middle and bottom cells were measured through 530 and 630 nm cut-on filters, respectively. All the component cells were light-soaked in the open-circuit mode and the temperature was maintained at 50 °C.

Figure 14 plots the power output for the component cells versus light soaking time. We have also plotted the light soaking data for our previously reported component cells (Xu et al. 1993). It is clear from the figure that the cells with high hydrogen dilution not only exhibit better initial performance but also retain higher stabilized power. All the component cells in this study show true saturation after prolonged light exposure. The normalized degradation for the improved top and middle cells are 8.9% and 16.7%, respectively, compared to 11% and 18% reported previously. Note that the improved bottom cell shows the tendency of saturation in a shorter time than the previous sample. There is very little degradation beyond 200 hours of light soaking for the improved bottom cell. The stabilized power of 3.6 mW/cm^2 measured through a 630 nm cut-on filter after over 1000 hours of light soaking is the highest reported to-date for a-SiGe:H alloy bottom cells.

To obtain a 15% stable module efficiency, Guha (Guha et al. 1994) has estimated that a 16% stabilized small-area cell efficiency is necessary. In Table 22, we list the previously established stabilized cell performances from our laboratory, the results from this study, and the values for reaching the 16% goal. One can see from Table 22 that the difference between the present status and the goal are mainly in the following two areas: (1) V_{oc} in both the top and the middle cells, and (2) FF for the middle and the bottom cells. The two major challenges are therefore the enhancement in V_{oc} of ~100 mV for the top and the middle cells and the further improvement in the quality of the a-SiGe:H alloy. These challenges can be met only by innovative material research and device design with focused effort. In addition, if one can

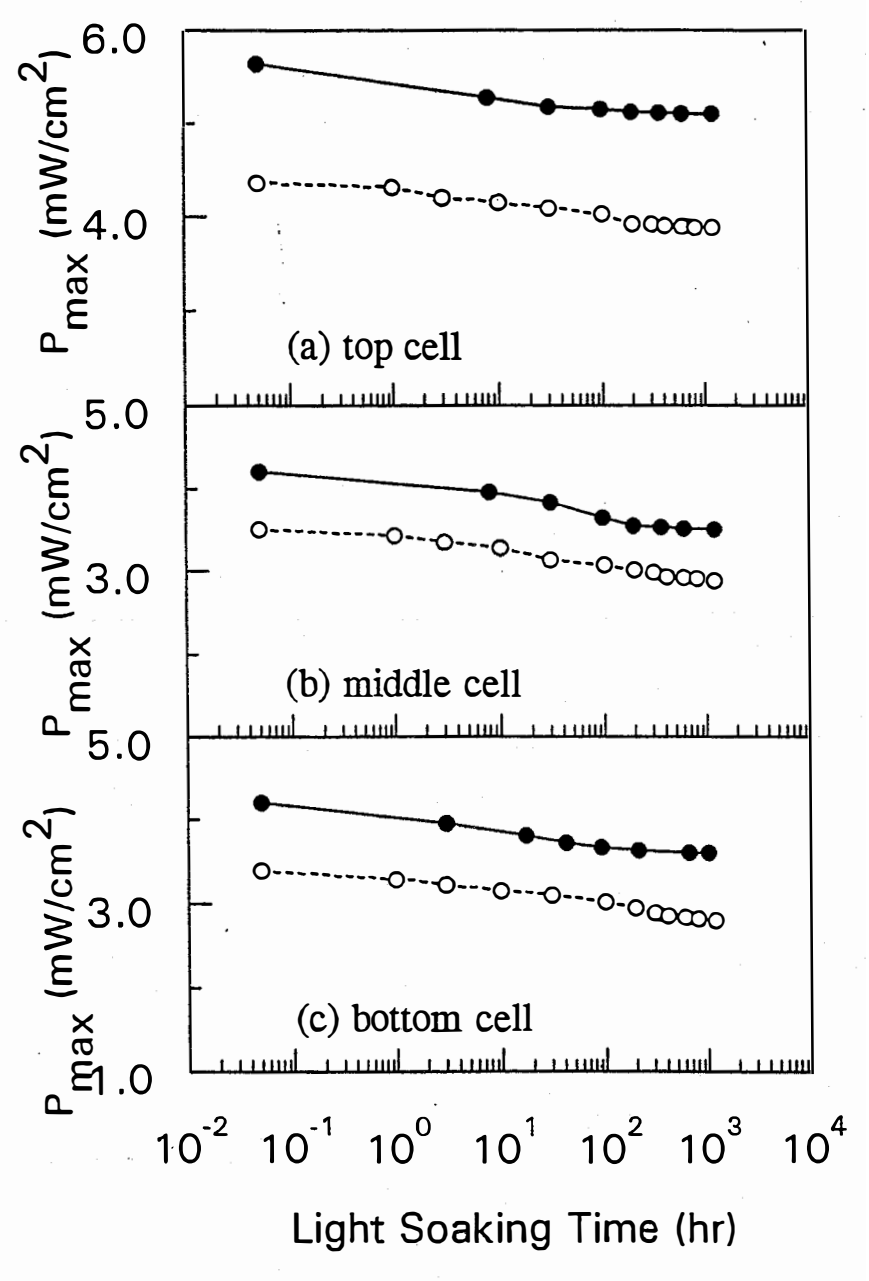

Figure 14. Previously reported (O) and improved (●) stability data for the (a) top, (b) middle, and (c) bottom component cells.

further improve the quality of the back reflector by eliminating or reducing its parasitic loss, the requirement for the bottom cell can be relaxed. One may then either use a thinner *i* layer for higher FF or incorporate a smaller amount of Ge for higher V_{oc}. The degree of back reflector texture also plays a role in the stability of the cell as discussed in detail by Banerjee et al. (Banerjee et al. 1994).

Table 22. Previous and Present Stabilized Component Cell Status at United Solar. Parameters for 16% goal are also listed.

Component Cell	Status	J_{sc} (mA/cm²)	V_{oc} (V)	FF	P_{max} (mW/cm²)
Top*O	Previous	7.2	0.98	0.71	5.0
	Present	7.3	0.97	0.72	5.1
	Goal	8.2	1.10	0.75	6.8
Middle*▲	Previous	6.9	0.74	0.57	2.9
	Present	7.6	0.76	0.60	3.5
	Goal	8.4	0.89	0.70	5.2
Bottom†□	Previous	7.7	0.65	0.56	2.8
	Present	9.8	0.66	0.55	3.6
	Goal	8.6	0.68	0.68	4.0

* deposited on textured substrate coated with Cr
† deposited on textured Ag/ZnO
O measured under AM1.5
▲ measured under AM1.5 with a $\lambda > 530$ nm filter
□ measured under AM1.5 with a $\lambda > 630$ nm filter

Status of Triple-junction Devices

As discussed above, we have achieved improved component cells using high hydrogen dilution during film growth. We have started to incorporate these component cells into triple-junction configuration and obtained some promising results.

The characteristics of two triple-junction a-Si:H alloy solar cells in both initial and degraded states are listed in Table 23. The cells were measured by a single-source solar simulator. The initial efficiency is around 13%. These triple cells degraded by 12 to 14% after 600 hours of light soaking in an open-circuit mode at 50 °C, maintaining a stable efficiency of 11.0 ~ 11.1%. These cells were sent to NREL for triple-source measurement, and the results are also listed in Table 23. The highest total-area efficiency measured by NREL was 9.97%. Considering the shadow-loss due to grids, this corresponds to an active-area efficiency of 10.8% which is in close agreement to the measured value with the single-source simulator. Optimization of triple-junction cells, including "tunnel" junctions and the component cell current matching, is in progress. Our best cell using hydrogen dilution to date shows 13.3% of efficiency in the initial state (see Table 23).

Table 23. Characteristics of Triple-Junction a-Si:H Alloy Cells in Initial and Degraded States.

Sample No.	State	η (%)	J_{sc} (mA/cm²)	V_{oc} (V)	FF	Q (mA/cm²) Top	Middle	Bottom
L7358	Initial	13.0	7.16	2.45	0.74	7.16	7.20	8.38
	Degraded	11.1	6.87	2.38	0.68	6.98	6.87	7.97
	NREL[1]	9.93	6.25	2.38	0.67			
	NREL[2]	10.8	6.75	2.38	0.67			
L7361	Initial	12.9	7.15	2.45	0.74	7.15	7.15	8.35
	Degraded	11.0	6.90	2.38	0.67	6.97	6.90	8.04
	NREL[1]	9.97	6.30	2.38	0.67			
	NREL[2]	10.8	6.79	2.38	0.67			
L7466	Initial	13.3	7.36	2.45	0.74	7.38	7.36	8.31

[1] Total-area, [2] Calculated active-area

Status of Cell Efficiency for Different Structures

The current status at United Solar in terms of initial and stable cell (0.25 cm² area) efficiencies for different single-, double- and triple-junction structures is shown in Table 24. For each of these structures,the stable efficiencies represent the highest reported in the literature. There are several points worth considering. There is a gain from 8.8% to 11.2% as we go from a single-junction to a multijunction, multibandgap structure. Use of Ge in the bottom cell improves the efficiency from 10.1% to 11.2%. We should note that at this point in time, there is no difference in the stabilized efficiencies between double- and triple-junction cells. As explained earlier, optimization of the triple-cell structure is still continuing, and a higher efficiency is expected with the current component cell performance. Moreover, a small improvement in the quality of a-SiGe alloy will have a much greater impact on increasing the stable efficiency of a triple-junction cell. In order to improve the efficiency of the double-junction cell further, the top cell thickness would have to increase to an extent that light-induced degradation will play a major role. The potential for improving the triple-cell efficiency is, therefore, much higher. In fact, computer simulations indicate that using realistic stabilized material parameters, the triple-junction approach is the only way to reach 15% efficiency and beyond.

Table 24. Highest Stable Cell Efficiencies at United Solar for Different Junction Configurations.

		J_{sc} (mA/cm^2)	V_{oc} (V)	FF	η (%)	Deg.
a-Si:H	Initial	15.25	0.94	0.72	10.3	
	Degraded (600 hrs)	15.12	0.91	0.64	8.8	14.6%
a-Si:H/a-Si:H	Initial	7.9	1.89	0.76	11.4	
	Degraded (1000 hrs)	7.9	1.83	0.70	10.1	11.4%
a-Si:H/a-SiGe:H	Initial	10.67	1.65	0.72	12.6	
	Degraded (600 hrs)	10.61	1.61	0.66	11.2	11.1%
a-Si:H/a-SiGe:H/ a-SiGe:H	Initial	7.16	2.45	0.74	13.0	
	Degraded (600 hrs)	6.87	2.38	0.68	11.1	14.6%

Section 9

Future Directions

Considerable progress has been made in the performance of the component cells of the multijunction structure, and a stable small-area efficiency of 12% is expected to be achieved when the triple-junction cells are suitably optimized. Further improvement in efficiency would need development of better materials especially in terms of stability. As seen in Table 22, considerable reduction in the degradation of a-SiGe:H alloy cells will be necessary to meet the desired bottom cell performance. The stability problem in thick a-Si:H alloy cells demands the use of Ge in the middle cell to obtain the desired current density. This reduces V_{oc}, and the performance, therefore, is poorer. New deposition regimes/methods will play a key role in the development of better materials. There have been many reports of improvement of material performance by using new deposition processes. In almost all these cases, the improvement is associated with a reduction in defect density as measured by CPM. As discussed extensively in this report, CPM is not adequate to ascertain the suitability of a material for optimum solar cell performance. It is therefore essential that new methods of material growth must be accompanied by corresponding experiments on the material using a device configuration. This would necessitate collaborations amongst different laboratories, and a good beginning has already been made under the Thin-film Partnership program.

Another area of enormous potential is the optimization of the back reflector. We have discussed earlier that there is an unidentified parasitic loss at the Ag/ZnO and/or ZnO/Si interface. Experiments with alternative conducting oxide/nitrides will be useful to address this issue. Development of a two-dimensional optical model will also guide the experimentalist to design optimum textures for light trapping.

References

Arch, J.K., Rubinelli, F.A., Hou, J.Y., and Fonash, S.J. (1991). *J. Appl. Phys.*, Vol. 69, p. 7057.

Arya, R.R., Catalano, A., and Oswald, R.S. (1986). *Appl. Phys. Lett.*, Vol. 49, p. 1089.

Banerjee, A., Yang J., Glatfelter, T., Hoffman K., and Guha, S. (1994). *Appl. Phys. Lett.*, Vol. 64, p. 1517.

Banerjee, A., Yang, J., Hoffman, K., and Guha, S. (1994). *Appl. Phys. Lett.*, Vol. 65, p. 472.

Banerjee, A., Hoffman, K., Xu, X., Yang, J., and Guha, S. (1994). *First World Conference on Photovoltaic Energy Conversion Proc.; December 5-9, 1994; Waikoloa, Hawaii*; p. 539.

Banerjee, A. (1995). *Solar Energy Materials and Solar Cells,* Vol. 36, p. 295.

Banerjee, A., Xu, X., Yang, J., and Guha, S. (to be published 1995). *Mat. Res. Soc. Proc.*; Spring 1995, San Francisco, California.

Cabarrocas, P. Roca i., Morin, P., Chu, V., Conde, J.P., Liu, J.Z., Park, H.R., and Wagner, S. (1991). *J. Appl. Phys.*, Vol. 69, p. 2942.

Chen, I. and Wronski, C.R. (to be published). *J. Non-Cryst. Solids.*

Cuniot, M. and Marfaing, Y. (1988). *Philos. Mag.*, Vol. B 57, p. 291.

See, for, example, Curtins, H. and Favre, M. (1989). *Amorphous Silicon and Related Materials, Vol. A.* Edited by H. Fritzsche (Advances in Semiconductors, Vol. 1, World Scientific Publishing Co., Singapore, 1989) p. 329.

Delley, B. and Steigmeier, E.F. (1993). *Phys. Rev.*, Vol. B47, p. 1397.

Doughty, D.A., Doyle, J.R., Lin, G.H., and Gallagher, A. (1990). *J. Appl. Phys.*, Vol. 67, p. 6220.

Drevillion, B. and Toulemonde, M. (1985). *J. Appl. Phys.*, Vol. 58, p. 1.

Evangelisti, F. (1985). *J. Non-Cryst. Solids*, Vol. 77&78, p. 969.

Fantoni, A., Vicira, M., and Martins, R. (1994). *Mat. Res. Soc. Proc.*, Vol. 336, p. 711.

Ganguly, G. and Matsuda, A. (1994). *Mat. Res. Soc. Proc.*, Vol. 336, p. 7.

Ganguly, G., Nishio, H., and Matsuda, A. (1994). *Appl. Phys. Lett.*, Vol. 64, p. 3581.

Guha, S., Narasimhan, K.L., and Pietruszko, S.M. (1981). *J. Appl. Phys.*, Vol. 52, p. 859.

Guha, S., Yang, J., Nath, P., and Hack, M. (1986). *Appl. Phys. Lett.*, Vol. 49, p. 218.

Guha, S., Yang, J., Jones, S.J., Chen, Y., and Williamson, D.L. (1992). *Appl. Phys. Lett.*, Vol. 61, p. 1444.

Guha, S., Yang, J., Banerjee, A., Glatfelter, T., Hoffman, K., Ovshinsky, S.R., Izu, M., Ovshinsky, H.C., and Deng X. (1994). *Mat. Res. Soc. Proc.*, Vol. 336, p. 645.

Guha, S., Yang, J., Banerjee, A., Glatfelter, T., Hoffman, K., and Xu, X. (1994). *Solar Energy Materials and Solar Cells*, Vol. 34, p. 329.

Guha, S., Xu, X., Yang, J., and Banerjee, A. (to be published 1995). *Mat. Res. Soc. Proc.*; Spring 1995, San Francisco, California.

Hazra, S., Middya, A.R., and Ray, S. (1995). *J. Appl. Phys.*, Vol. 78, p. 581.

Kane, E.O. (1961). *Phys. Rev.*, Vol. 127, p. 131.

Knights, J.C., Lucovsky, G., and Nemanich, R.J. (1978). *Philos. Mag.*, Vol. B37, p. 467.

Knights, J.C., Lucovsky, G., and Nemanich, R.J. (1979). *J. Non-Cryst. Solids*, Vol. 32, p. 393.

Lee, S., Arch, J.K., Fonash, S.J., and Wronski, C.R. (1990). *Twenty-First IEEE PVSC Proc.*; May 21-25, 1990, Orlando, Florida; p. 1624.

Matsuura, H. and Okushi, H. (1992). *Amorphous & Microcrystalline Semiconductor Devices.* Edited by J. Kanicki, Artech House, Vol. II; p. 517.

Mimura, H. and Hatanaka, Y. (1987). *Appl. Phys. Lett.*, Vol 50, p. 326.

Perrin, J., Takeda, Y., Hirano, N., Matruura, H., and Matsuda, A. (1989). *Jpn. J. Appl. Phys.*, Vol. 28, p. 5.

Schropp, R.E.I., Ouwens, J.D., Von der Linden, M.B., Van der Werf, C.H.M., Van der Weg, W.F., and Alkemade, P.F.A. (1993). *Mat. Res. Soc. Proc.*, Vol. 297, p. 797.

Tanaka, K. and Matsuda, A. (1987). *Mat. Sci. Report*, Vol. 2, p. 139.

Turner, W.A., Jones, S.J., Pang, D., Bateman, B.F., Chen, J.H., Li, Y.M., Marques, F.C., Wetsel, A.E., Wickboldt, P., Paul, W., Bodart, J., Norberg, R.E., El Zawawi, I., and Theye, M.L. (1990). *J. Appl. Phys.*, Vol. 67, p. 7430.

Williamson, D.L. (to be published 1995) *Mat. Res. Soc. Proc.*; Spring 1995, San Francisco, California.

Xi, J., Liu, T., Iafelice, V., Si, K., and Kampas, F. (1994). *Mat. Res. Soc. Proc.*, Vol. 336, p. 681.

Xu, X., Yang, J., and Guha, S. (1993). *Appl. Phys. Lett.*, Vol. 62, p. 1399.

Xu, X., Yang, J., and Guha, S. (1993). *Twenty-Third IEEE PVSC Proc.*; May 10-14, 1993, Louisville, Kentucky; p. 971.

Yang, J., Ross, R., Glatfelter, T., Mohr, R., Hammond, G., Bernotaitis, C., Chen, E., Burdick, J., Hopson, M., and Guha, S. (1988). *Twentieth IEEE PVSC Proc.*; Sept. 26-30, 1988, Las Vegas, Nevada; p. 241.

Yang, J., Xu, X., and Guha, S. (1994). *Mat. Res. Soc. Proc.*, Vol. 336, p. 687.

Yang, J., Banerjee, A., Glatfelter, T., Hoffman, K., Xu, X., and Guha, S. (1994). *First World Conference on Photovoltaic Energy Conversion Proc.; December 5-9, 1994; Waikoloa, Hawaii*; p. 380.

REPORT DOCUMENTATION PAGE

Form Approved
OMB NO. 0704-0188

1. AGENCY USE ONLY (Leave blank)	2. REPORT DATE	3. REPORT TYPE AND DATES COVERED
	October 1995	Annual Subcontract Report, 1 August 1994 - 31 July 1995

4. TITLE AND SUBTITLE
Amorphous Silicon Research
Phase I

5. FUNDING NUMBERS
C: ZAN-4-13318-02
TA: PV431301

6. AUTHOR(S)
S. Guha

7. PERFORMING ORGANIZATION NAME(S) AND ADDRESS(ES)
United Solar Systems Corp.
Troy, Michigan

8. PERFORMING ORGANIZATION REPORT NUMBER

9. SPONSORING/MONITORING AGENCY NAME(S) AND ADDRESS(ES)
National Renewable Energy Laboratory
1617 Cole Blvd.
Golden, CO 80401-3393

10. SPONSORING/MONITORING AGENCY REPORT NUMBER
TP-411-20205
DE95013124

11. SUPPLEMENTARY NOTES
NREL Technical Monitor: W. Luft

12a. DISTRIBUTION/AVAILABILITY STATEMENT

12b. DISTRIBUTION CODE
UC-1262

13. ABSTRACT *(Maximum 200 words)*

This report describes the process made during the first year of a three-year research program to improve our understanding and capabilities for the development of multijunction hydrogenated amorphous silicon (a-Si:H) alloy cells and modules. Highlights of the work include (i) investigation of new deposition regimes/conditions such as hydrogen and He dilution, triode configuration, etc., (ii) fundamental studies to obtain the bandgap of microcrystalline p layer used in high-efficiency solar cells and band-edge discontinuity at the microcrystalline and amorphous interface, (iii) development of new techniques to analyze bulk and interface losses in solar cells, and (iv) development of high-efficiency single- and multijunction cells. The highest stable active-area cell efficiencies for different cell structures were achieved using hydrogen dilution during deposition and are as follows: (1) a:Si:H single-junction—8.8%, (2) a-Si:H/a-Si:H same gap double-junction—10.1%, (3) a-Si:H/a-SiGe:H dual gap double-junction—11.2%, (4) a-Si:H/a-SiGe:H/a-SiGe:H triple gap triple-junction—11.1%. All these results are the highest reported in the literature.

14. SUBJECT TERMS

15. NUMBER OF PAGES
60

16. PRICE CODE

17. SECURITY CLASSIFICATION OF REPORT	18. SECURITY CLASSIFICATION OF THIS PAGE	19. SECURITY CLASSIFICATION OF ABSTRACT	20. LIMITATION OF ABSTRACT